JOINT EUROPEAN TORUS

JET–P(92)16

P.E. Stott
and JET Team

The Development of Plasma Measurement Techniques and their Impact on Fusion Research

The Development of Plasma Measurement Techniques and their Impact on Fusion Research

P.E. Stott
and JET Team*

JET-Joint Undertaking, Culham Science Centre, OX14 3DB, Abingdon, UK

** See Annex*

Preprint of Paper to be submitted for publication in
Reports on Progress in Physics

ABSTRACT.

The development of measurement techniques for magnetically-confined fusion plasmas is reviewed. The past decade has seen the introduction of several new techniques as well as significant improvements of existing methods. In most cases these developments have had a direct effect on progress in improving the performance of fusion plasmas and in understanding their behaviour.

Contents

1. Introduction

The goal of fusion research is the controlled release of energy from the nuclear reactions between light nuclei, particularly the reactions between the heavier isotopes of hydrogen, deuterium and tritium,

$$d + t \Rightarrow {}^4He + n + 17.6\ MeV.$$

Fusion reactions can take place only if the nuclei are brought close together and the gaseous fuel must be heated to a very high temperature in order for a significant number of nuclei to have sufficient energy to overcome the Coulomb repulsive force. The reaction between deuterium and tritium requires temperatures in the range 10 keV $< T_i <$ 20 keV (1 keV $\approx$ 10 M°C), which is several times hotter than the centre of the sun.

At these temperatures the fuel is a *fully ionized plasma* and must be thermally insulated from its material surroundings. The effectiveness of the thermal insulation is conveniently expressed by the *global energy confinement time* τ_E, which is the characteristic exponential decay time of the plasma kinetic energy when all sources of heating are removed. Initially an external heating source is needed to raise the plasma to the required temperature, but the fusion power increases as the temperature is raised. One fifth of the fusion power is released in the alpha particles (He^4) and retained to heat the plasma. In a thermal plasma with equal parts of deuterium and tritium, the plasma heating by the alpha particles will balance the energy losses so that the fusion reaction will become energetically self-sustaining, when the triple product of the plasma ion density, the energy confinement time and the ion temperature, $n_i \tau_E T_i \approx 5 \times 10^{21}\ m^{-3}$skeV.

There are two alternative routes to obtain the required combination of temperature, density and confinement time. One route is *inertial confinement* where a solid fuel pellet is heated and compressed by lasers or particle beams to extremely high densities ($n_i \approx 10^{31}\ m^{-3}$) and confined for very short times ($\tau_E \approx 10^{-11}$ s) by the inertia of the compressed pellet. The other route is by *magnetic confinement* where lower density plasmas ($n_i \approx 10^{20}\ m^{-3}$) are confined for longer times ($\tau_E >$ 1 s) by strong magnetic fields. The most promising magnetic confinement systems are *toroidal* and of these the furthest advanced is the *tokamak* (figure 1). This combines a strong *toroidal magnetic field*, produced by external coils, with a weaker *poloidal field*, produced by a current flowing in the plasma. Other toroidal magnetic confinement systems differ in the details of the magnetic fields. They include *stellarators* where

the poloidal field is produced by external coils and *pinches* where the poloidal field is much stronger than the toroidal field.

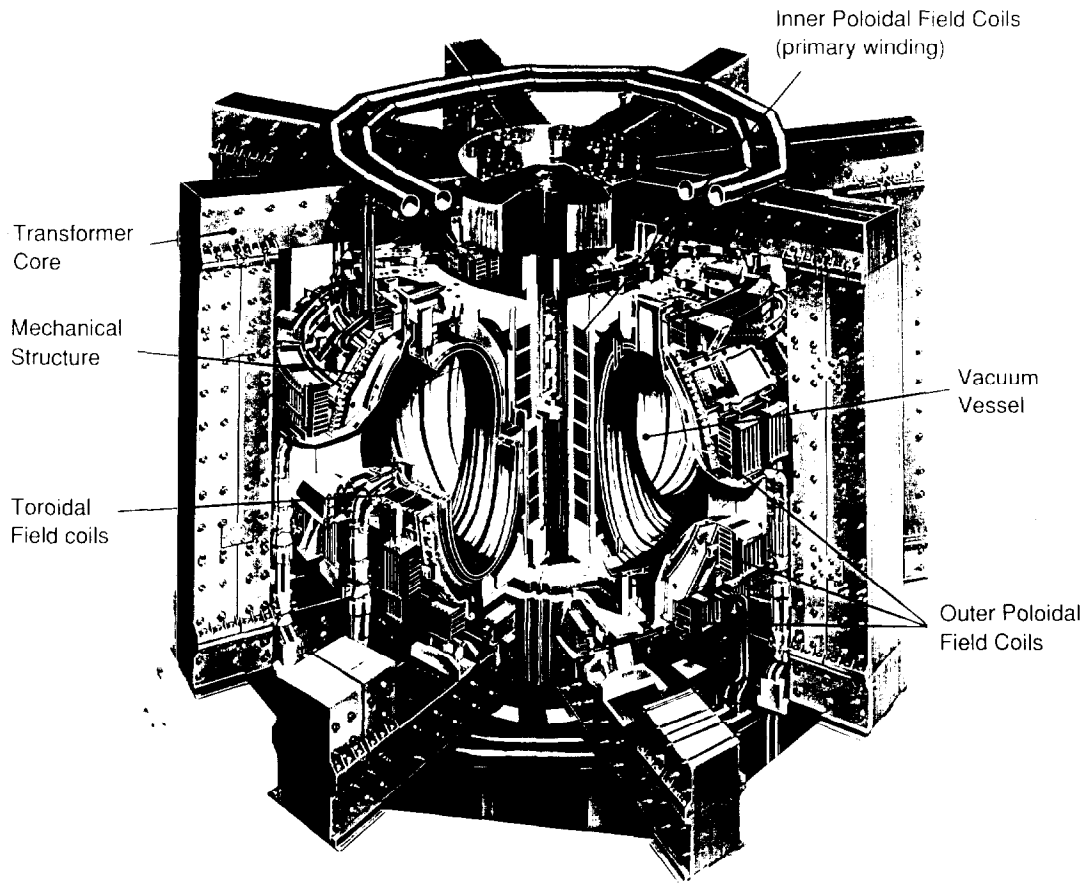

Figure 1: Schematic of the world's largest tokamak, the Joint European Torus (JET), showing the principal components.

Present-day magnetic confinement experiments are usually carried out in hydrogen or deuterium plasmas. The fusion reactions between two deuterons (there are two branches with equal probabilities),

$$\begin{aligned} d + d &\Rightarrow {}^{3}He + n + 3.27\ MeV \\ d + d &\Rightarrow t + p + 4.03\ MeV \end{aligned}$$

require an even higher temperature than the d-t reaction. As these reactions produce much lower fluxes of neutrons than a mixture of deuterium and tritium at the same temperature, they are conveniently used to explore the confinement regimes relevant to fusion without the added difficulties of producing large fluxes of neutrons that would activate the experimental structures.

Fusion research has made considerable progress in recent years both in extending plasma performance and in understanding specific phenomena. Since 1970, the fusion triple product has increased by four orders of magnitude

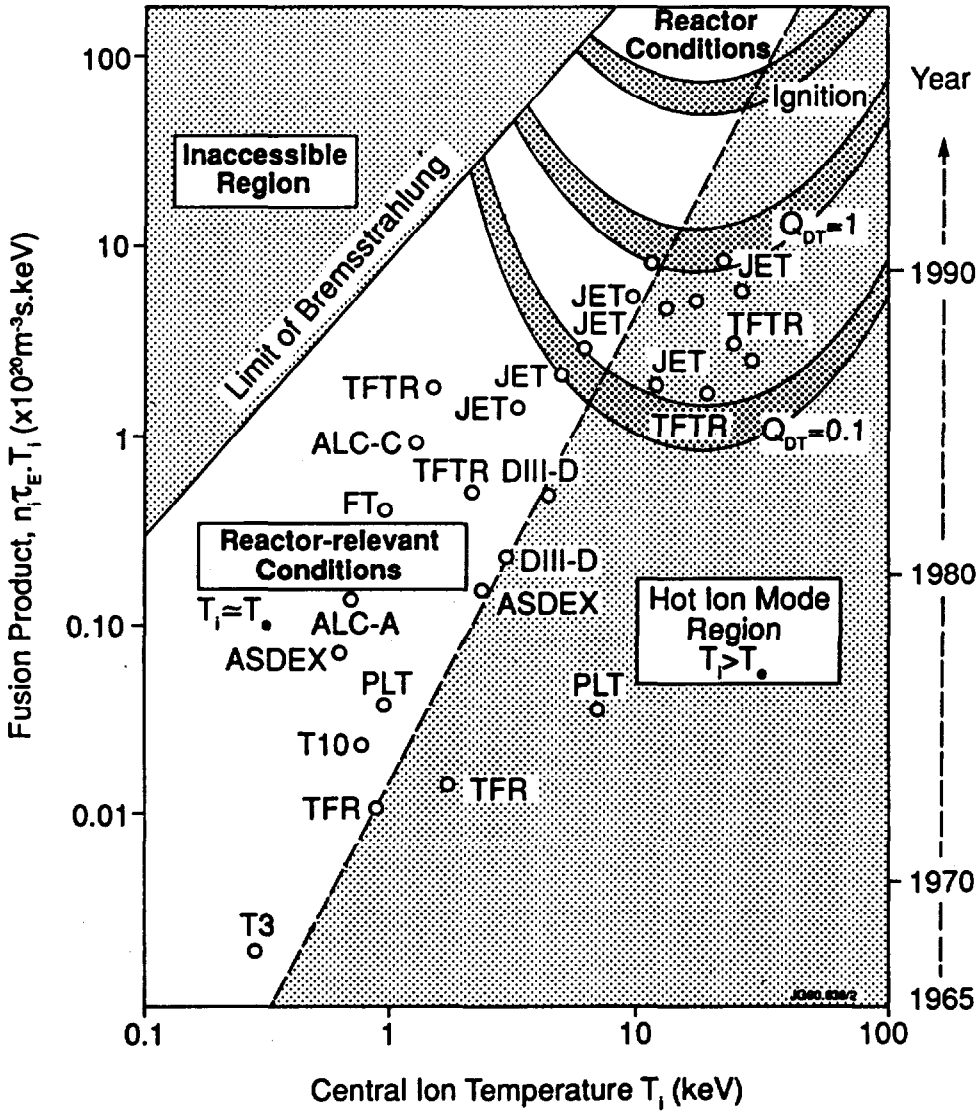

Figure 2: The fusion triple product (density x energy confinement time x temperature versus central ion temperature) for various experiments, showing the considerable progress that has been made.

(figure 2) and is now very close to the range required for a fusion reactor. Values for JET have increased from $n_i \tau_E T_i \approx 6 \times 10^{19}$ m^{-3}skeV and $T_i \approx 2.6$ keV in 1985 to $n_i \tau_E T_i \approx 9.5 \times 10^{20}$ m^{-3}skeV and $T_i \approx 28$ keV in 1991.

A preliminary series of experiments with a relatively low concentration of tritium (10%) in a deuterium plasma has been carried out in JET during 1991 and has produced over 1.5 MW of fusion power (The JET Team 1992). If these experiments were to be repeated with 50% tritium in the best JET plasma conditions, the total fusion power would be about 10 MW and approximately equal to the power invested to heat the plasma. More extensive experiments with tritium are planned for later phases of the programmes for JET and for the american tokamak TFTR. To reach ignition will require a tokamak with linear dimensions approximately two to three times larger than JET. The

International Thermonuclear Experimental Reactor (ITER) project will be an international collaboration involving the CEC, USA, Russia and Japan. The detailed engineering design is expected to start during 1992.

2. Diagnostic Requirements

Fusion research requires the measurement of many plasma quantities. Because there are large differences in densities, dimensions and time scales between inertially- and magnetically-confined plasmas, quite different measurement methods have been developed and it would be difficult to cover both fields in a single review. Therefore this review will deal only with diagnostics for magnetic confinement and moreover will concentrate on tokamak diagnostics, although many of the techniques can be applied to other magnetic confinement geometries. There are several general reviews of plasma diagnostics (Equipe TFR 1978, Orlinskiy and Magyar 1988). A series of reviews of the different areas of diagnostic methods will be found in the proceedings of the series of courses on plasma diagnostics held by the International School of Plasma Physics in Varenna (Sindoni and Wharton 1978, Stott *et al* 1982, 1986 and 1991). These proceedings also contain useful references to the many detailed papers which have been published in the scientific journals. A recently published book by Hutchinson (1987) explains the underlying physics of some diagnostic methods and a book by Wesson (1987) provides an excellent introduction to the physics of tokamaks.

Magnetic confinement experiments are usually pulsed for times ranging from a few tenths of a second in small experiments to several seconds in larger experiments. A typical sequence is shown in figure 3. The plasma is characterized by a range of macroscopic parameters such as the size, shape and position of the plasma, the total plasma current (I_p), the total kinetic energy (W_p) and the global energy confinement time (τ_E). These macroscopic quantities are usually measured throughout the duration of the plasma pulse with a time resolution that is short compared to the time scale of changes in the equilibrium. Usually this requires measurements on a time scale of 10^{-4} to 10^{-2} s. On a similar time scale, measurements are made of spatially distributed quantities such as the current density and the densities and temperatures of the plasma ions and electrons. In a stable tokamak plasma, these quantities usually have toroidal and poloidal symmetry and are conveniently characterized by spatial profiles that cut across all the magnetic surfaces. Profile shapes can range from broad profiles that are flat (or even hollow) in the core of the plasma with steep gradients at the edge, to profiles that are strongly peaked in the core. Profile measurements require

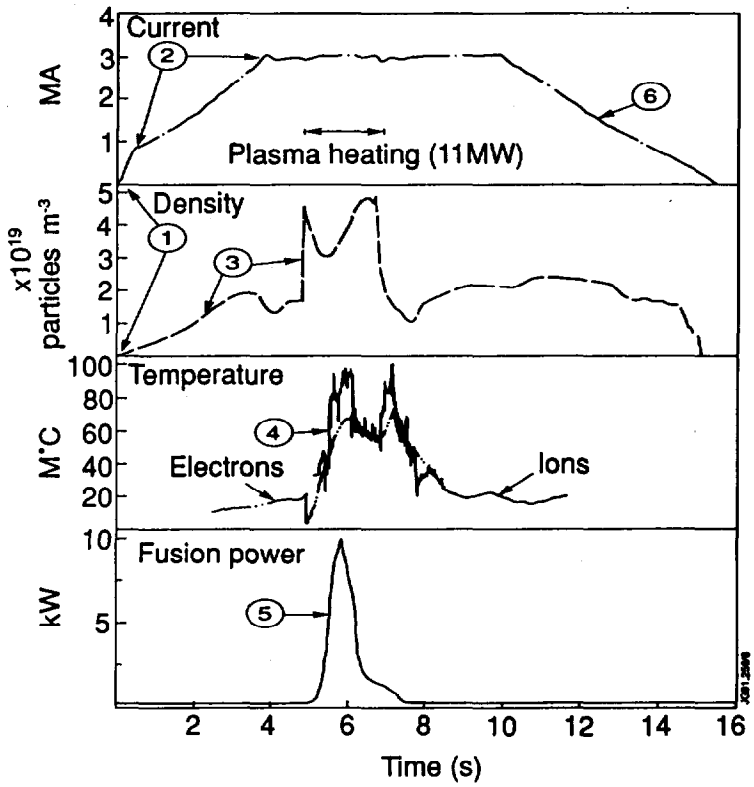

Figure 3: A typical sequence for a tokamak experiment: (1) The plasma is formed by ionizing a small quantity of deuterium gas; (2) the plasma current is raised progressively to the required value, in this case 3 MA, and held constant for several seconds; (3) the plasma density is raised, by adding more gas and by firing in high velocity pellets of deuterium ice; (4) the plasma temperature is raised by a combination of ion cyclotron and neutral beam heating; (5) the fusion power peaks at the time when the product of density and temperature is maximized.

spatial resolution capable of resolving the shortest scale length and this usually corresponds to a few percent of the overall dimensions of the plasma. Measurements of fluctuations in plasma temperatures, densities and other parameters are made on much faster time and shorter spatial scales to study instabilities in the plasma. For many years it has been postulated that high frequency fluctuations may be responsible for enhanced plasma energy transport and there have been extensive efforts to develop diagnostics that can resolve fluctuations with small amplitudes and scale lengths.

Measurements in high temperature fusion plasmas are usually difficult because methods involving physical contact with the plasma can be used only in cool plasmas at the extreme edge. Non-invasive methods must be used for all measurements in the hot, dense plasma core. These include *passive* methods utilizing radiation or particles that have been emitted spontaneously by the plasma, and *active* methods using radiation or particles from an external source to probe the plasma. A wide variety of measurement techniques is

employed. Some techniques can measure more than one plasma quantity, and some plasma quantities can be measured by different techniques. It is particularly desirable to be able to measure the most important plasma parameters by several independent methods whenever possible. Some techniques work only over a limited range of plasma conditions and thus different diagnostic systems may be needed to cover the complete range encountered in a particular experiment. Some techniques cannot be absolutely calibrated and may need to be cross-calibrated against other methods. Most measurement techniques depend on complex plasma effects whose interpretation may be difficult, particularly in some ranges of plasma operation, and thus it is always desirable to be able to compare the results from independent measurement methods.

2.1 Diagnostic overview

In attempting to review diagnostics in a systematic way, they can be grouped either according to the measurement technique or according to the plasma quantity ("parameter") that is to be measured. Both approaches have some merits, but also some limitations as neither approach can be followed completely systematically without repetition. The main part of this review will classify the diagnostics by technique, but for the benefit of readers who may be new to the subject, this section will provide a brief overview of the main plasma quantities that are measured, with a comparison of the different diagnostic methods.

The total plasma current and the shape and position of the plasma boundary are usually determined by measurements of the external magnetic fields, although occasionally other methods are used. Estimates of the shape of internal magnetic flux surfaces can be inferred from external field measurements combined with additional information and assumptions about plasma profiles, but the precision is poor in the core region where the spatial profile of the plasma current density is very important for plasma stability and studies of the detailed power balance. Several diagnostic methods to measure internal magnetic fields have been developed including *polarimetry, Thomson scattering* and by *spectroscopic emission from atomic beams.*

The density of electrons is measured with *transmission interferometry, reflectometry* or *Thomson scattering.* These methods are well developed and used for measurements of spatial profiles and of localized fluctuations. Impurity ion densities are measured with various spectroscopic methods including passive *line emission spectroscopy* and active *charge–exchange spectroscopy.* The effective ion charge $Z_{eff} = \sum_i Z_i^2 n_i / n_e$ (where the summation is taken over

all charge states of all impurity species) is a useful quantity to characterize the purity of a plasma and ranges from $Z_{eff} = 1$ in pure hydrogen to $Z_{eff} = 6$ in pure carbon. Z_{eff} can be calculated from the measured impurity ion densities, but is more easily and reliably measured from the enhancement of the bremsstrahlung continuum in a spectral region free from strong emission lines. The density of hydrogenic (ie. fuel) ions, which is an important quantity as it appears in the fusion triple product, is not easily measured directly but can be derived if the impurity ion densities are known. The deuterium ion density n_D is calculated by comparing neutron flux (proportional to $n_D^2 T_i^m$ where $3 < m < 5$) and ion temperature measurements.

In low- and medium-density plasmas, the ions and electrons can have significantly different temperatures. Electron temperature profiles are measured with *Thomson scattering, electron cyclotron emission* and *soft X–ray emission.* The last two techniques are also used to measure electron temperature fluctuations with high spatial and time resolution. Several techniques are used to measure ion temperature profiles, including *neutral particle emission, charge–exchange recombination spectroscopy, X–ray crystal spectroscopy* and *neutron diagnostics.* All of these techniques have some limitations so that ion temperatures are generally measured with more difficulty than electron temperatures.

The global plasma energy balance requires measurements of the total plasma kinetic energy and the total power input and losses. The total plasma energy can be derived by integrating the spatial profiles of ion and electron densities and temperatures over the plasma volume or a global value can be determined from the reaction of the plasma on the external magnetic fields (the vertical magnetic field and the diamagnetic effect on the toroidal field). The power applied to heat the plasma is determined in various ways: (i) the ohmic power is easily calculated from the plasma current and the restive part of the voltage drop around the torus (both of these quantities are measured magnetically); (ii) the global power inputs from neutral beam and radio frequency heating are measured by various calorimeter and radio frequency techniques. The total power lost from the plasma by impurity radiation is measured using arrays of bolometers with broad spectral response, viewing the plasma through small apertures so as to make a pin-hole camera. The plasma transport coefficients can be determined from localized power and particle balances but many of the quantities required are not directly measured and must be calculated using models from other measured quantities. Transport coefficients are also determined by observing the response of the density and temperature profiles to perturbations.

In many ways the edge plasma is more difficult to diagnose than the core. Spatial scale lengths are dominated by atomic processes and are usually independent of the overall dimensions of the plasma. Moreover there are usually significant toroidal and poloidal asymmetries. Until quite recently the edge plasma has received rather less priority than the core and consequently edge diagnostics are less well developed. *Langmuir probes* are used to measure density, temperature and power flux at the extreme edge where temperatures are sufficiently low. *Infra–red imaging* is used to measure power fluxes to material surfaces. Impurity deposition and erosion are measured with *collector probes* and fluxes into the plasma are measured *spectroscopically.* There is a difficult gap between the region of plasma that can be diagnosed by these edge techniques and the core diagnostics.

The neutrons and fusion products that are the end result of the fusion process can be measured with various instruments adapted from nuclear physics. These techniques also provide measurements of many other plasma quantities.

2.2 Data recording and analysis

In the earliest days of fusion research, waveforms were displayed on banks of oscilloscopes and recorded on 35mm film. The introduction of polaroid film allowed data to be reviewed more promptly, but still it was necessary to measure signal heights off the film (usually by hand, although a few digitizing scanners were in use). Accuracy was poor and it was tedious and time consuming to analyze more than a few channels of data at different time slices during a discharge. One of the most important developments to influence plasma measurements during the last decade has been the introduction of computerized data acquisition methods.

Electronic data acquisition methods have advanced rapidly, allowing the signals from many channels to be recorded at many time points. With these advances the rapid reduction and analysis of raw data is possible with the result that many plasma quantities which previously were laborious to calculate by hand and were therefore evaluated for only a few selected times in a few "typical" discharges, are now calculated automatically and displayed for every discharge. This is of particular benefit in setting up and optimizing the plasma conditions. Some plasma measurements are incorporated in feedback loops to control the values of important plasma quantities such as the current, shape, position and density. The capability of fast micro-processors is developing rapidly and opening up exciting prospects for real-time data analysis. This ability to record large quantities of data has

brought problems of data management, so that it is usually necessary to apply some strict rules in establishing well-managed data bases.

3. Magnetic Measurements

Many of the macroscopic parameters of a magnetically-confined plasma including the shape, position, current, loop-volts, ohmic power input, plasma pressure and kinetic energy may be derived from electrical or magnetic measurements (Stott 1982a, Wootton 1991, Braams 1991). These are the most fundamental of the wide range of techniques applied to fusion experiments. The basic methods have not changed substantially, though there has been a considerable development in the sophistication of the implementation and instrumentation. The measurements of plasma shape, position and current are particularly important for the safe operation of a large experiment and these diagnostics are now usually incorporated into feedback control loops.

3.1 Magnetic topology of the tokamak

The tokamak magnetic confinement system has two main components (figure 4). The stronger component is the *toroidal field* B_t (typically in the range 1 to 10 Tesla). This field is usually produced by external coils and it varies inversely with the *major radius* R. Thus $B_t(R) = B_o R_o/R$ where B_o is the field at the toroidal axis R_o. It is not usually necessary to measure the vacuum

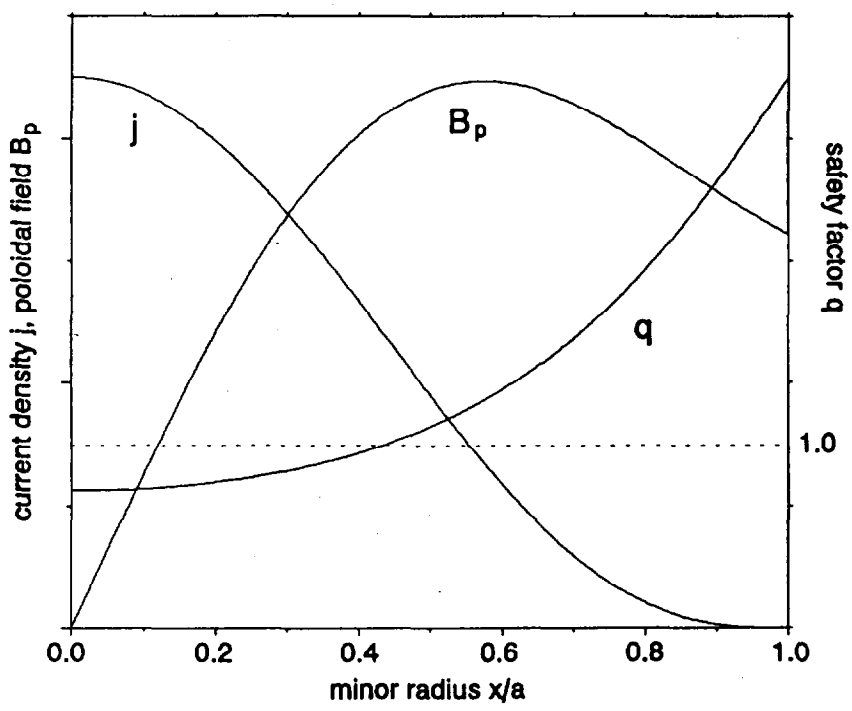

Figure 4: Components of the tokamak magnetic field system (Soltwisch 1991)

toroidal field in a tokamak as it is quasi-stationary and easily computed from the toroidal coil current. However a small amount of the toroidal flux is excluded by the plasma by the *diamagnetic effect.* This measurement is used to determine the *poloidal beta* (β_p) which is the ratio of the plasma pressure to the pressure of the poloidal magnetic field. This is an important quantity in stability theory. The total kinetic energy due to particle velocities perpendicular to the toroidal field can be derived from the diamagnetic measurement. The small diamagnetic flux change is measured by integrating the transient voltage induced in a coil wound around the plasma. The diamagnetic measurement is simple in principle but notoriously difficult in practice due to the many large-amplitude and spurious induced voltages which must be carefully subtracted from the measured voltage.

The weaker component of the tokamak confinement system is the *poloidal field* B_p ($B_p/B_t \approx 0.1$). This is produced by a current I_p through the plasma in the toroidal direction. Typical values of I_p range from 10 kA in small tokamaks up to 7 MA in JET. The total plasma current is measured by electronically integrating the voltage induced in a *Rogowski* coil. This consists of a uniformly wound solenoid which is bent around the torus in the poloidal direction, with one end of the solenoid connected back through its center in order to cancel the voltage induced by the toroidal field. The loop-voltage V_ℓ is measured with a single turn of wire passing toroidally around the tokamak. Under steady state conditions these two quantities give the *ohmic power input,* $P_{OH} = I_p V_\ell$, and the *plasma resistance,* $\mathcal{R}_p = V_\ell / I_p$, which depends on the plasma temperature and purity.

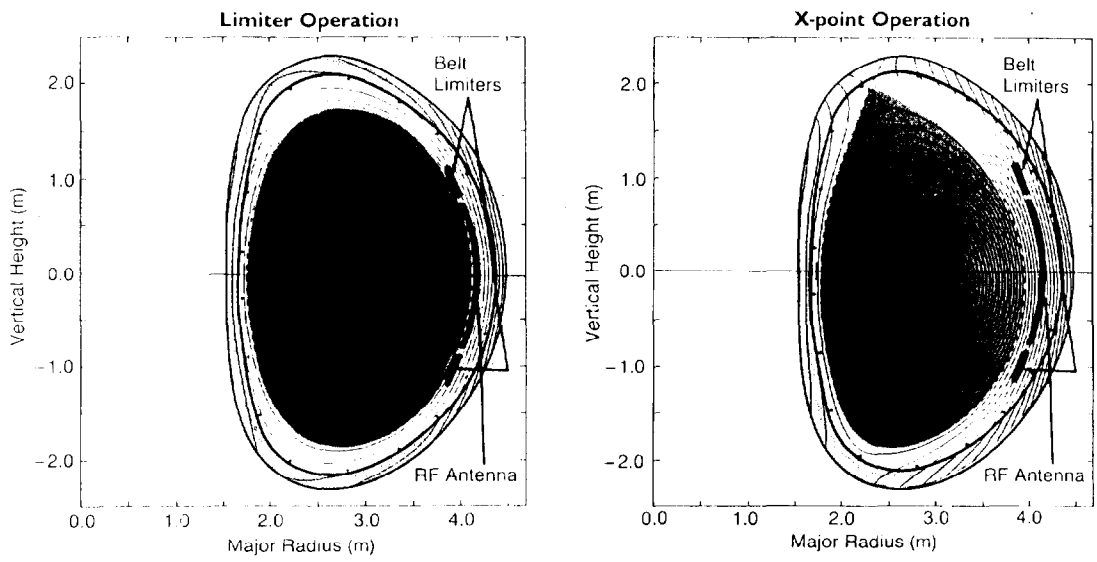

Figure 5: The tokamak magnetic fields form an infinite set of nested magnetic fields in a) limiter and b) divertor configurations.

The poloidal field is modified by external coils which produce additional vertical and radial fields to position and shape the discharge. The complete magnetic field forms a set of nested, toroidal *magnetic flux surfaces.* The plasma edge may be defined by either a *limiter* or a *divertor.* In the first configuration (figure 5a) a material limiter intersects the outermost flux surfaces, whilst in the divertor configuration (figure #5b) the outermost magnetic surfaces are modified so that they intersect a specially protected section of the vacuum vessel wall.

3.2 Plasma shape and position

The shape and position of the plasma boundary are determined by measuring the poloidal magnetic field outside the plasma. A typical arrangement is shown in figure 6. The small solenoidal coils measure the component of B_p parallel to the wall of the torus and the larger saddle coils measure the perpendicular

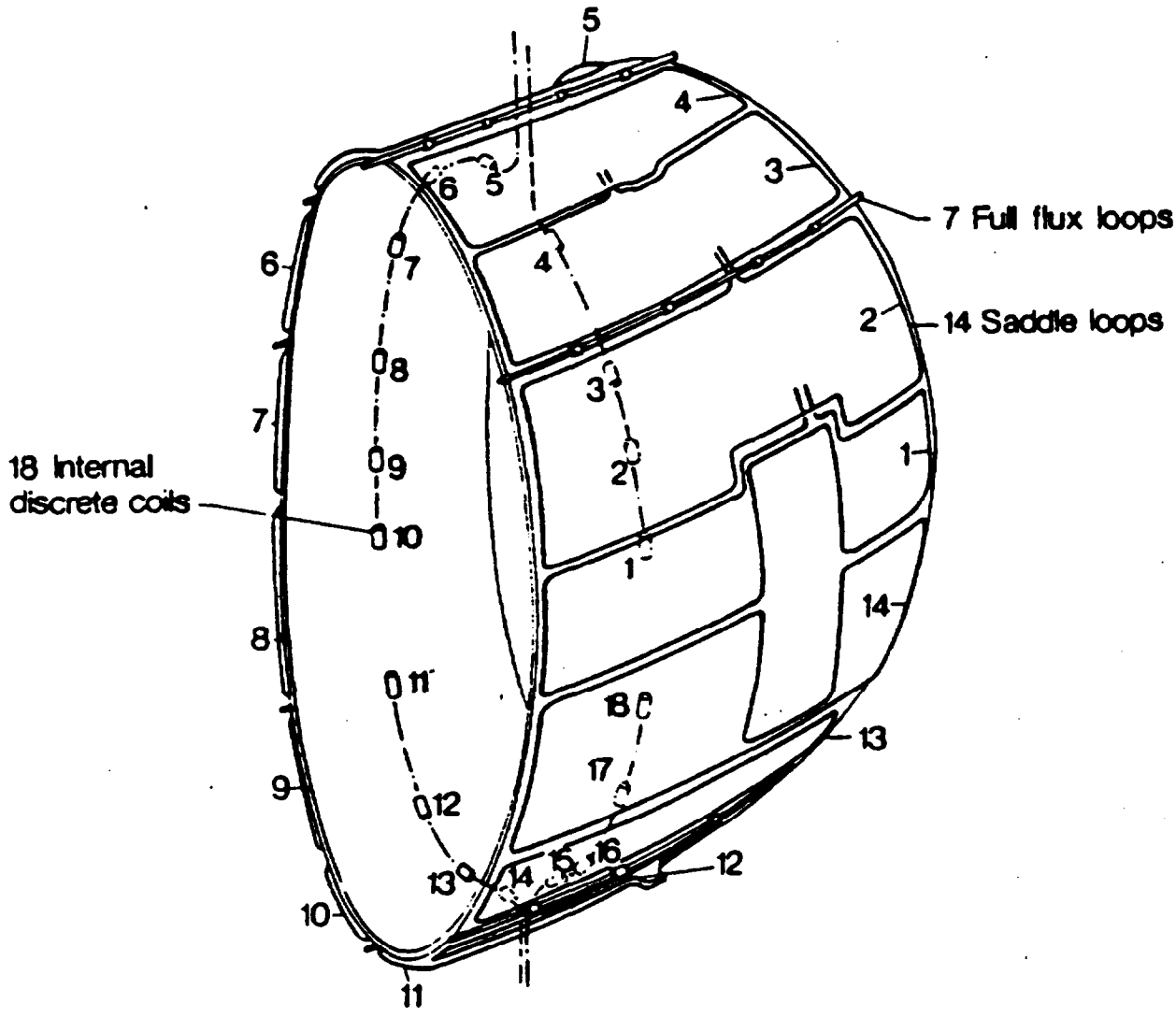

Figure 6: Arrangement of magnetic sensor coils in the JET tokamak.

component. The shape and location of the outermost closed magnetic flux surface which defines the plasma boundary is determined by solving Maxwell's equations for the magnetic field in the vacuum region outside the plasma. With this technique the shape of the plasma boundary in JET (poloidal dimensions 2.5 m by 4.2 m) is determined to within ±5 mm. The internal flux surfaces can be estimated by solving model equations for the plasma equilibrium. In small tokamaks with large aspect ratio (R/a) and circular poloidal cross-section, the plasma position can be measured rather simply with pairs of small pick-up coils at the inside/outside and top/bottom of the plasma. Rogowski-type coils with variable pitch windings proportional to the sine or cosine of the poloidal angle have been used (Wootton 1979) to measure the Fourier components of the external fields. These components can be related directly to the plasma position, ellipticity, triangularity etc.

3.3 The safety factor q(r)

The magnetic field lines follow a gentle helical path on a magnetic flux surface as they go around the torus. The *pitch* of the magnetic field on each surface is characterized by the *safety factor q*. Confusion can be caused by a number of slightly different definitions of q. The most precise value, $q_\psi = \oint (B_t/2\pi R B_p)ds$, where the integral is taken over a single poloidal circuit around the flux surface, is usually referred to as the *flux surface q*. For a flux surface with circular poloidal cross-section of *minor radius* r and large aspect ratio R_0/r, there is the approximate expression $q_{cyl} = rB_t/R_0B_p$. The value of $q(a)$ (also denoted as q_a) at the plasma boundary, $r = a$, is easily determined from external magnetic measurements. It is much more difficult to determine the profile $q(r)$ in the interior of the plasma. Estimates can be obtained from the external magnetic measurements, but the uncertainties for $r \ll a$ are large. Other diagnostic methods including polarimetry, Thomson scattering and injected atomic beams will be discussed later.

3.4 Magnetic perturbations

The safety factor $q(r)$ is so-called because of the role it plays in determining the *stability* of the plasma. If $q = m/n$ where m and n are integers, a field line joins up on itself after m toroidal and n poloidal transits around the torus. A perturbation of the form $\exp i(m\theta - n\varphi)$, where m and n are the poloidal and toroidal *mode numbers* and θ and φ are the poloidal and toroidal angles, is resonant on the *rational magnetic surface* $q = m/n$. Magnetohydrodynamic (mhd) theory predicts that such perturbations can be

unstable under certain conditions. Mhd activity within the plasma perturbs the equilibrium magnetic fields and can be detected with magnetic pick-up coils (often called *Mirnov coils*) located outside the discharge. The mode numbers m and n are determined from the phase differences between coils at different toroidal and poloidal positions. In the example shown in figure 7 (Fishpool 1992), the plasma current is increasing with time and thus q(a) is falling. Bursts of magnetic activity with $m/n \approx$ q(a) appear as q(a) passes through successive rational values. Usually these perturbations rotate around the torus and thus appear as oscillations to the fixed detection coils. Sometimes the perturbations stop rotating (Snipes *et al* 1988) and may lock in a particular toroidal phase so that they appear as quasi-stationary perturbations to the detector coils. Special care is required to monitor the presence of these "locked modes" which may continue to grow in amplitude although they are no longer rotating.

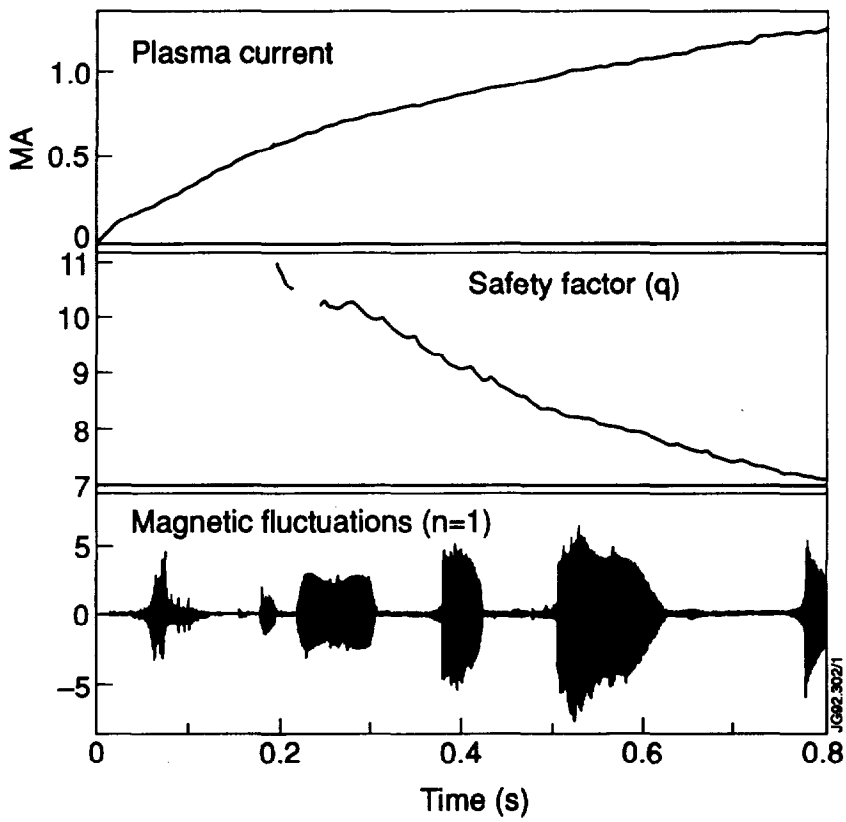

Figure 7: Bursts of instabilities grow as q at the plasma edge passes through rational values during the current rise (Fishpool 1992)

3.5 Disruptions

If q(a) is too small (there is a soft limit at q_ψ(a) $\approx$ 3 and a hard limit at q_ψ(a) $\approx$ 2), or if the plasma density is too large, the plasma current is terminated catastrophically in a *disruption.* Magnetic diagnostics play an important role in detecting the perturbations that precede the disruption. A

critical feature is the $m = 2$, $n = 1$ mode which substantially changes the magnetic topology within the plasma. The simple nesting of the toroidal magnetic flux surfaces is broken and *magnetic islands* appear. The position and dimensions of the islands can be estimated from the magnetic measurements. The effect of islands on plasma quantities such as the temperature will be discussed later. The value of $q(0)$ in the core of the plasma is important for studies of the *sawtooth* instability which will be discussed in a later section.

4. Microwave and Infra-red Transmission Techniques

4.1 Transmission interferometry

Interferometry with electromagnetic waves at millimeter and sub-millimeter wavelengths is one of the methods used to measure electron densities. The phase of a wave that has passed through the plasma is compared with a reference wave that has propagated for a similar distance in free-space. This is one of the longest-established diagnostic methods, but there have been many significant technical developments as the simple, single-channel microwave interferometers used on the earliest fusion experiments have evolved into the sophisticated multi-chord, far infra-red systems that are now standard instrumentation on most tokamaks (Veron 1982, Soltwisch 1991). Present-day fusion experiments are equipped with feedback control systems to assist reproducible operation. Data from interferometers play an important role in controlling the plasma density through feedback systems that regulate the gas admission and in protecting the vessel through systems that inhibit the powerful beam heating sources from operating if the plasma density is too low.

The general expression for the refractive index of a magnetized plasma is a complicated function of the *electron density* n_e, the vector *magnetic field* **B** and the *frequency* f of the propagating wave. When the wave is *ordinarily polarized* (the electric vector of the wave is parallel to **B**) the refractive index, $\mu = (1 - n_e e^2/4\pi^2 f^2 \varepsilon_0 m_e)^{0.5}$, depends only on the wave frequency and the electron density. The wave cannot propagate if the electron density exceeds the *critical density* $n_c = 4\pi^2 f^2 \varepsilon_0 m_e e^{-2} = 1.24\times10^{-2} f^2$, where n_c is in m^{-3} and f is in Hz. For many applications $n_e \ll n_c$ and thus $\mu \approx 1 - n_e/2n_c$, so that the *phase difference* $\Delta\phi$ between the beam that has passed through the plasma and the reference beam depends on the line integral of the electron density,

$$\Delta\phi = (2\pi/\lambda)\int(1 - \mu)dl \approx \frac{e^2}{4\pi\varepsilon_0 cfm_e}\int n_e(r)dl = 2.82\ 10^{-15}\int n_e(r)dl.$$

4.1.1 Phase modulation. A simple Mach-Zehnder interferometer has two serious limitations for plasma applications. First the measurement is sensitive to the amplitudes of the two beams and thus is easily perturbed by changes in the source amplitude or in the attenuation of the beam in the plasma. Secondly it is not easy to determine if the plasma density is increasing or decreasing because the sign of the phase change is not determined uniquely. These limitations are avoided by modulating the phase of the reference beam and constructing a second, reference interferometer without any plasma in its measurement beam (figure 8). The phase shift is determined by comparing the sinusoidal signals from the two interferometers and measuring the time interval between corresponding zero crossings. This measurement is independent of the amplitudes of the two signals and also the sign of the phase shift is determined uniquely. The modulation frequency is determined by the required time resolution. Frequency shifts up to about 10^5 Hz, corresponding to a time resolution of about 10^{-4} s, can be produced by Doppler shifting the reference beam using a moving mirror or a rotating cylindrical grating (Veron 1982). Increased time resolution has been obtained using the beat frequency between two separate sources.

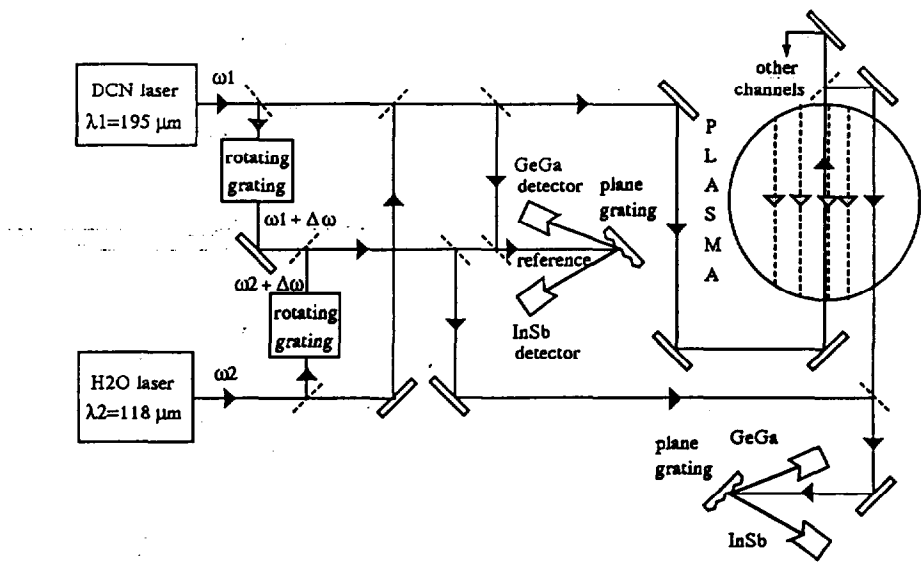

Figure 8: Principle of the Tor Supra interferometer system which has five measurement channels. Each channel has two interferometers operating at different wavelengths to allow compensation for mechanical vibrations. Each interferometer contains a reference arm whose phase is modulated relative to the plasma beam in order to determine the phase shift (Bruneau and Gil 1991).

4.1.2 Limits on the probing frequency. The choice of the probing frequency is influenced by several factors. The wave must propagate in the plasma and thus the frequency must be above the cut-off frequency $f_c = 8.98 \times 10^3 \, n_e^{0.5}$ (units are Hz and m^{-3}) for the maximum electron density along the line of sight. Microwave interferometers with $150 < f < 300$ GHz can be used for $n_e < 10^{20}$ m^{-3} provided that the beam passes close to the centre of the plasma where

refraction is small. Even at densities below the cut-off, beams along chords further from the centre can be refracted by the density gradient sufficiently to miss the exit window. In multi-chord interferometers a more stringent limit on frequency is set by refraction than by cut-off. This usually makes it necessary to work at higher frequencies in the far infra-red. Suitable sources are hydrogen cyanide ($f = 8.9 \times 10^{11}$ Hz, $\lambda = 337$ μm), deuterium cyanide ($f = 1.54 \times 10^{12}$ Hz, $\lambda = 195$ μm), methyl alcohol ($f = 2.52 \times 10^{12}$ Hz, $\lambda = 119$ μm) and water vapour ($f = 2.50 \times 10^{12}$ Hz, $\lambda = 118$ μm) lasers.

The upper limit on frequency is determined by the required resolution of the interferometer. The measured phase shift is sensitive to physical changes in the optical path caused by mechanical vibrations of the optical components in the interferometer. These effects can be minimized by careful mechanical design. Ideally the optical components should be mounted on a strong and rigid frame that is well damped and decoupled from sources of vibration such as the magnetic structure of the fusion device. Even with these precautions the amplitude of vibrations cannot be reduced easily below about 10 μm. This sets an effective upper frequency limit of about 3×10^{12} Hz ($\lambda \approx 100$ μm). Higher frequencies can be used, or the mechanical design simplified for interferometers at lower frequencies, by adding a secondary interferometer operating at a different (usually higher) frequency which is more sensitive to mechanical changes in the optical path but less sensitive to the plasma. This technique was applied in the DIII experiment (Baker and Lee 1978) with a carbon dioxide laser ($\lambda = 10.6$ μm) combined with a helium-neon laser ($\lambda = 0.633$ μm). The interferometer on the Tore Supra tokamak uses a combination of deuterium cyanide ($\lambda = 195$ μm) and water vapour ($\lambda = 118$ μm) lasers to correct for the effects of mechanical vibrations (Bruneau and Gil 1991). The temporal evolution of the uncompensated signals from the two interferometers and the compensated signal due to the plasma density are shown in figure 9.

4.1.3 Density profile measurements. In the early applications of interferometry as a fusion plasma diagnostic, a single measurement was made, usually along a plasma diameter, allowing a mean density to be evaluated from the measured line-integral density divided by the plasma chord length. Modern interferometers make simultaneous measurements of the line-integral densities along several chords through the plasma in order to determine the spatial profile of the density by a simplified form of tomographic inversion known as Abel inversion. This assumes that the density is constant on each magnetic flux surface. For non-circular plasmas this requires a knowledge of the shape of the magnetic flux surfaces, usually from magnetic diagnostics. One widely

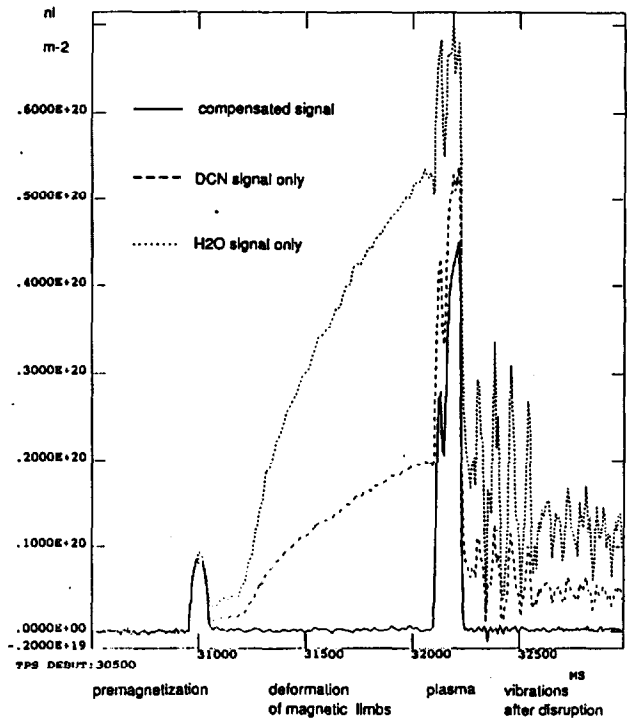

Figure 9: Temporal evolution of the Tor–Supra interferometer system showing the effect of vibrations on the two measurement channels and the resulting compensated plasma density signal (Bruneau and Gil 1991).

used technique reconstructs a three-dimensional density distribution by piling up thin disks and adjusting their dimensions and displacements to match the measured phase shift profile (Gottardi 1979).

Multi-chord, far infra-red interferometers based on these principles have evolved in two directions. Most systems use discrete optics for each chord and the number of chords is limited (typically to fewer than 10 chords) by the complexity and number of optical components. A further limitation on many fusion experiments, particularly the larger ones, is the number of vacuum ports that can be allocated to one diagnostic system. The number of measurement chords in these systems is too small to resolve the finer structure of density profiles or to resolve small-scale density fluctuations. An alternative approach to multi-chord interferometry is to expand a single beam to illuminate the whole cross-section of the plasma. This greatly reduces the number of optical components and permits better spatial resolution. This technique is particularly well-suited to smaller fusion experiments where the whole plasma cross-section can be viewed through a single access port. Systems based on the beam expansion method have been used in the TEXT tokamak (Kim *et al* 1988a) and in several other experiments. The high spatial resolution has been important in a variety of fluctuation studies and in determining transport coefficients from the propagation of density perturbations. The TEXT

system is being extended to have two orthogonal views, each with expanded beam and multiple detectors. The increasing sophistication of interferometer systems is illustrated by the scanning multi-view interferometer (figure 10) based on a multi-sectored blazed grating that has been developed by Howard (1989) for the H-1 heliac experiment.

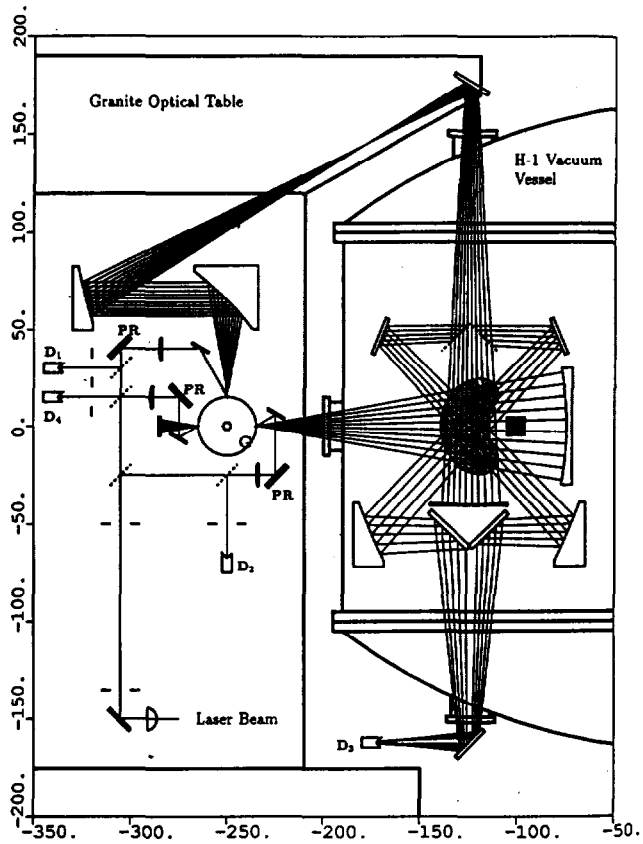

Figure 10: Conceptual design of an interferometer for the H-1 heliac experiment. Local oscillator arms are not shown (Howard 1989).

4.2 Polarimetry

The polarization of an electromagnetic wave changes as it propagates through a magnetically-confined plasma. In a tokamak (where the toroidal field B_t is much stronger than the poloidal field B_p) this polarization change is reduced to a Faraday rotation caused by the poloidal field, if the frequency of the wave is much larger than the *electron cyclotron frequency* $f_{ce} = 2.8 \times 10^6 B_t$ (with f_{ce} in Hz and B_t in Tesla). This condition is satisfied in the far infra-red. The Faraday rotation angle is given by:

$$\alpha = \text{const } f^{-2} \int_{-z}^{+z} n_e(r) B_{p\parallel}(r) dz$$

where $B_{p\parallel}$ is the component of the poloidal field parallel to the measurement chord.

4.2.1 Far infra–red polarimetry. The polarization measurement of the product of density and poloidal field is conveniently combined with measurement of density by a far infra-red interferometer (Soltwisch 1986). The basic principle is shown schematically in figure 11. The polarization of the probing beam after passing through the plasma is slightly elliptical due to linear birefringence and the plane of polarization has been rotated relative to the initial polarization. The beam is combined with the reference beam at a beam combiner which is made of parallel, thin metal wires. There are two detector signals: one signal is insensitive to the polarization and gives the integral of plasma density along the appropriate chord; the other signal gives the Faraday rotation angle, α, which must be measured with a resolution of a few milliradians. The dependence of α on the product of n(r) and $B_{p\parallel}$ (the component of B_p parallel to the measurement chord) conveniently weights the integral to the plasma core where information on B_p is most valuable. A unique reconstruction of the poloidal magnetic field from the Faraday rotation measurements would require a large number of probing beams, but access to most tokamaks is severely restricted by the surrounding machine structure so that there is usually only a small number of beams. To invert the data it is usually assumed that the density is constant on a magnetic surface. The density profile is derived first by inverting the interferometer signals. The poloidal field is then derived by inverting the rotation angle data.

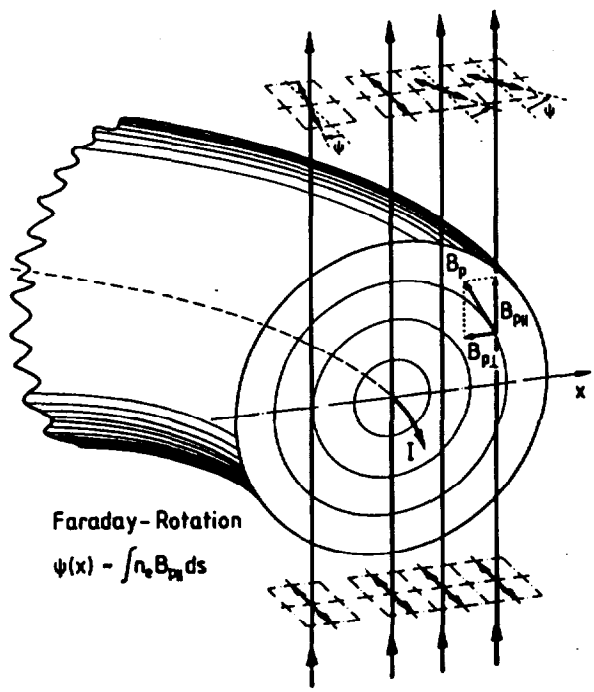

Figure 11: Basis of the polarimetry measurement (Soltwisch 1991)

4.2.2 Measurements of q(r). Polarimetry measurements on the Textor experiment (Soltwisch *et al* 1986) produced the unexpected result that $q(r \approx 0) < 1$ in the

plasma core (figure 12). Plasma theory had previously considered $q = 1$ to be a well-defined stability limit requiring $q > 1$ throughout the plasma. The widely observed *sawtooth instability* (discussed in more detail later), which causes a periodic loss of energy from the plasma core in most tokamaks, was thought to be triggered when $q = 1$. Recent data from JET show that $q(0)$ can be significantly less than unity ($0.6 < q(0) < 0.8 \pm 0.15$) and moreover there is only a small change in $q(0)$ at the time of the sawtooth instability. These results have stimulated a new appraisal of the magnetohydrodynamic stability theory of the core plasma. This provides a good example of the way that advances in fusion research are often stimulated by the development of new or improved diagnostics.

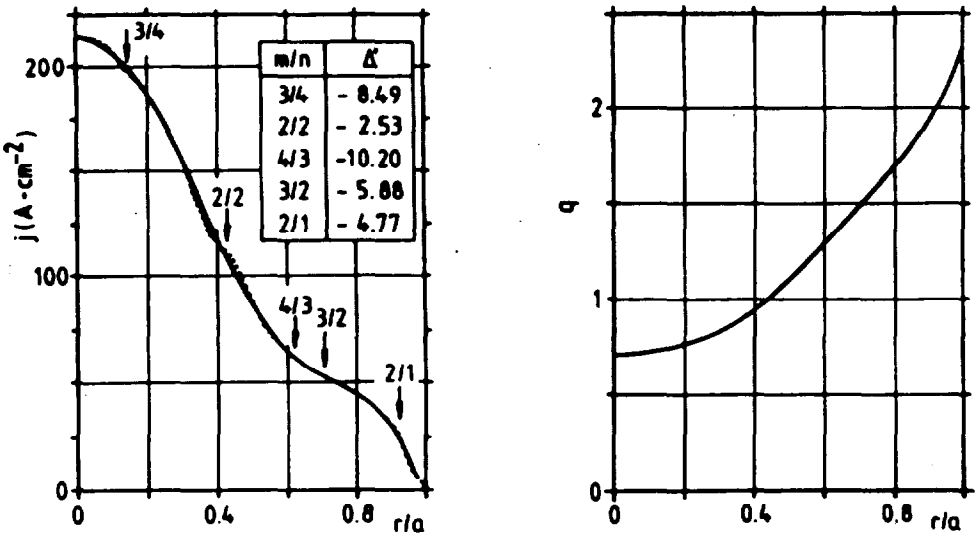

Figure 12: Profiles of: (a) the plasma current density, (b) the safety factor in TEXTOR (I_p = 476 kA, B_T = 1.7 T) (Soltwisch et al 1987).

4.3 Microwave reflectometry

Reflectometry differs from transmission interferometry in that the frequency of the electromagnetic probing beam is below the plasma frequency so that the wave is reflected at some point in the plasma. This technique was introduced as a diagnostic in some early tokamaks but was not fully developed until quite recently. Advances in microwave technology and a reappraisal of diagnostic requirements have stimulated a renewed interest (Costley 1986, 1991). A particular attraction of reflectometry is that it requires less access to the plasma compared to other density diagnostic techniques. The basic principle is simple and is well-known in atmospheric studies. An electromagnetic wave launched from an antenna at position R_a propagates into the plasma and is

reflected at the point R_c where the refractive index becomes zero. An ordinarily polarized wave of frequency f is reflected where the local electron density equals the critical density $n_c = 12.4 \times 10^{-3} f^2$, where n_c is in m^{-3} and f is in GHz. The phase delay of the wave is given by,

$$\phi = 4\pi \frac{f}{c} \int_{R_c}^{R_a} (1 - n_e(R)/n_c)^{0.5} dR - \pi/2.$$

This condition is derived by matching solutions of the wave equation at the reflecting layer. The term $\pi/2$ comes from the matching procedure at the plasma reflecting layer; the equivalent term for reflection at a metallic surface is π. The phase delay is measured by comparing the wave reflected from the plasma with a wave reflected from a mirror in an external reference path (figure 13). The phase can change in time due to three effects: (i) changes in the position of the reflecting layer; (ii) changes in the plasma density outside the reflecting layer; (iii) changes in the wave frequency.

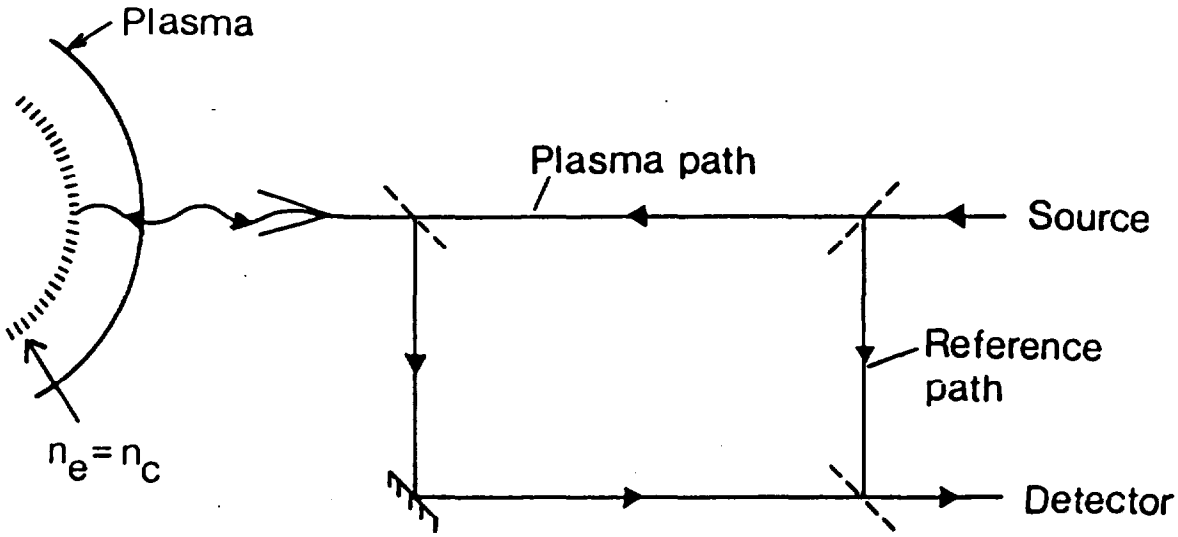

Figure 13: Principle of microwave reflectometry (Costley 1991).

4.3.1 Density profiles. The movement of the critical density layer is followed if the source frequency is fixed. The density profile is determined by sweeping the frequency. A reflectometer system was developed on the TFR experiment (Simonet 1985) using a backward-wave oscillator which could be swept in ≈ 5ms over the range 75 to 110 GHz corresponding to the density range 7×10^{19} to 1.5×10^{20} m^{-3}. Reflectometry is used as a density diagnostic on Tore Supra using three swept o-mode systems covering the ranges 22 to 35 GHz, 35 to 50 GHz, and 50 to 75 GHz and a single e-mode system covering the range 75 to 110 GHz. Broad-band swept-frequency reflectometers have been installed on several tokamaks and stellarators. For example, the ASDEX experiment employed two systems: one with three o-mode reflectometers (Manso *et al* 1991); and one e-mode reflectometer (Schubert *et al* 1990). These systems have been

used for a wide range of physics studies including measurements (figure 14) of the evolution of density profiles during the transition from the "L mode" to the "H mode". This is a regime of tokamak operation with improved energy confinement properties.

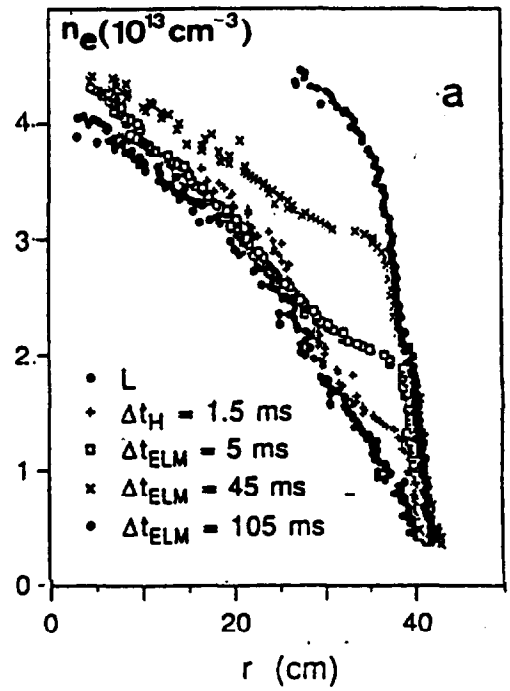

Figure 14: A sequence of reflectometry density profiles measured in ASDEX during the transition from the L to the H mode (Manso et al 1991).

It is difficult to apply the broad-band sweep technique to experiments where the sensitive components must be located at a large distance from the plasma. Oversized waveguides are required to minimize transmission losses and there are serious problems with standing waves and resonances which cannot be tuned out over a broad frequency range. These problems have been avoided in JET with a multi-channel reflectometer (Prentice *et al* 1986). This has twelve independent sources with frequencies between 18 and 80 GHz corresponding to densities in the range 4×10^{18} to 8×10^{19} m^{-3}. Each source can be swept over a narrow range (typically 100 MHz) to measure the density profile or it can be operated at a fixed frequency to measure density fluctuations. One application of this JET reflectometer is to study the coupling between particle and energy transport. This will be discussed in more detail in the section on electron cyclotron emission.

A new technique, similar to pulsed radar ranging, has been proposed recently (Heijnen *et al* 1991) to determine the position of the reflecting layer in the plasma. A short pulse of microwaves would be transmitted and the time delay until the pulse returns to the detector would be used to measure the position of the reflecting layer. This technique appears to be particularly interesting for future tokamaks with large spatial dimensions.

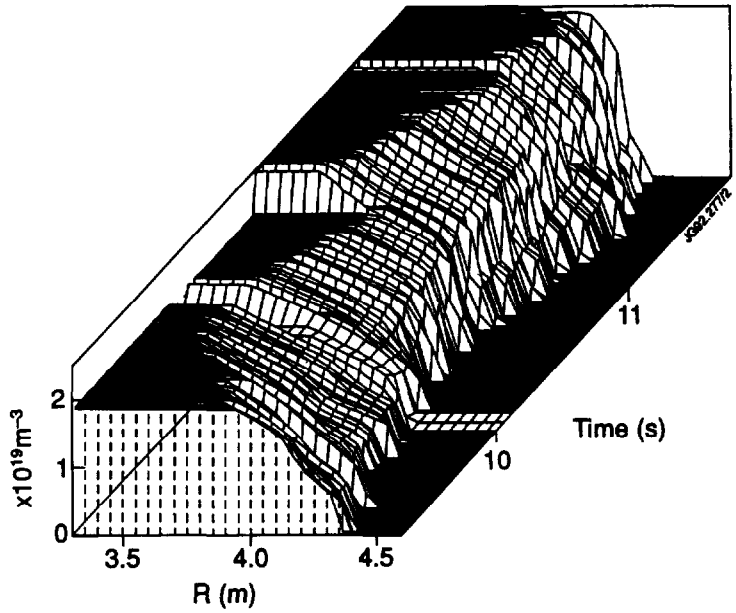

Figure 15: Edge density profiles in JET showing the transition from the L−mode to the H−mode.

4.3.2 Density fluctuations. One of the first attempts to apply reflectometry in a tokamak (Mazzucato 1975) was to measure the movement of the plasma as it was compression radially in the ATC experiment. Problems were encountered due to density fluctuations near to the reflecting layer. Density fluctuations scatter the reflectometer probing beam and add broad-band "noise" to the reflectometer signals at levels well above the system noise. Reflectometry is now beginning to be widely employed to study density fluctuations. Under suitable conditions there is good spatial localization to the region near to the reflecting layer. Figure 16 shows a typical application to studies of

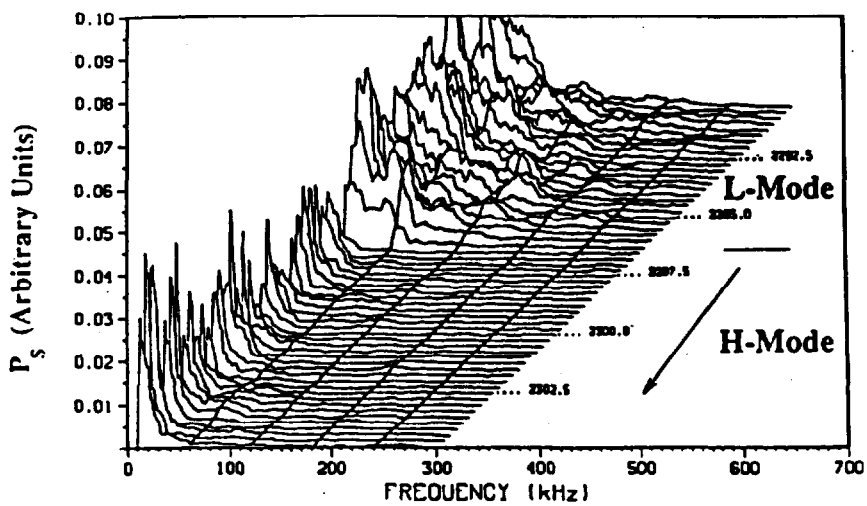

Figure 16: Temporal development of fluctuation spectra measured by reflectometry in the DIII−D experiment showing a reduction in the amplitude of fluctuations following the L−mode to H−mode transition (Peebles et al 1990).

fluctuations at the plasma edge in the DIII-D tokamak. These reflectometer measurements show a significant reduction in the amplitude of density fluctuations during the H-mode compared to the L-mode (Peebles *et al* 1990).

4.3.3. Magnetic field determination The refractive index depends on the magnetic field as well as on the electron density if the wave propagates in the e-mode (the extraordinary polarization where the electric vector of the wave is perpendicular to **B**). The density can be determined if the magnetic field is known independently. Alternatively simultaneous measurements of both polarizations, or the measurement of the density by some other independent method, offer the prospect of determining the local magnetic field (Costley *et al* 1990).

5. Microwave Emission

Electron cyclotron emission (ECE) was first studied as a possible energy loss mechanism in high-temperature fusion reactors but the diagnostic potential was quickly recognized. The fundamental principles of the method and its detailed application have been described by several authors (for example Costley 1982). Electrons gyrating in the confining magnetic field, emit electromagnetic radiation at the *electron cyclotron frequency* $f_{ce} = eB/2\pi m_e \approx 28xB$, (with f in GHz and B in Tesla) and at its low harmonics $f = nf_{ce}$, where $n \leq 4$. The cyclotron frequency in a tokamak plasma is determined mainly by the toroidal magnetic field which varies inversely with the major radius ($B_T \propto 1/R$), so that the *frequency* of the emitted radiation can be related directly to *spatial position* (figure 17). For a wide range of temperatures and densities the plasma emits as a black body in some harmonics and polarizations so that the *intensity* of the emission is simply related to the *electron temperature*. The time dependence of the temperature at a fixed point in the plasma is measured by observing the emission at the corresponding frequency. The complete emission spectrum in a suitable harmonic yields the spatial profile of the electron temperature $T_e(R)$. However, the inner part of the profile may be inaccessible due to the effect of harmonic overlap; when emission at one harmonic from the high field region at small major radius R, has the same frequency as a higher harmonic from the low field region at large R.

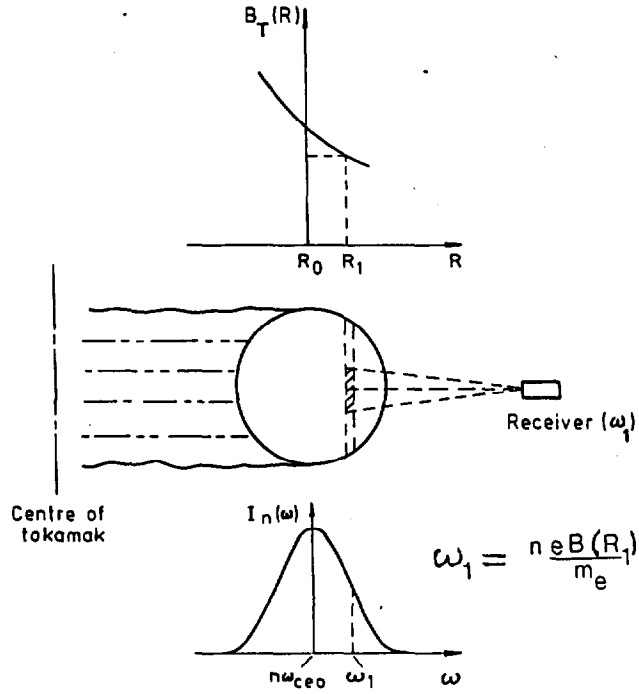

Figure 17: Frequency to space transformation illustrating the principle of the electron cyclotron emission diagnostic (Costley 1982).

5.1 Electron Cyclotron Emission detectors

The ECE spectrum from a tokamak with $2 < B_T < 8$ T is in the frequency range 60 to 600 GHz (ie. in the millimeter and sub-millimeter wave-bands). The full spectrum is conveniently measured with a *Michelson interferometer* (figure 18). The path difference within the interferometer is scanned rapidly and repetitively by moving one of the mirrors. In a typical system the mirror is vibrated mechanically at 50 Hz. The time resolution is about 10 ms and the frequency resolution is typically 10 GHz. Faster systems with resolution better than 1ms have been developed: by scanning the mirror pneumatically; by rotating an angled mirror; or by pulsing a plasma in the reference arm of the

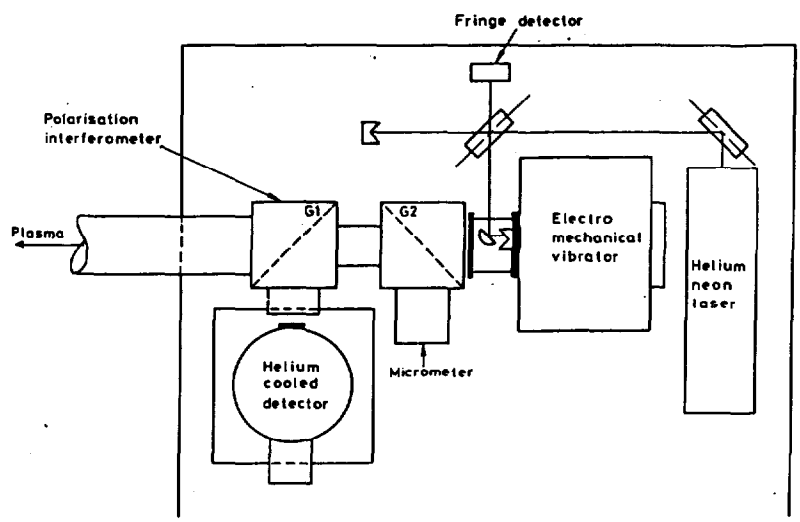

Figure 18: Schematic of a Michelson interferometer for *ECE (Costley 1982).*

interferometer. A subsequent Fourier transform of the recorded interference pattern yields the emission spectrum which can be related to the temperature profile.

A more limited spectral range, but with better time and frequency resolution, is covered by a *Fabry–Perot parallel–plate etalon* used as a tunable filter (figure 19). With a fixed plate separation, the emission at a fixed frequency can be used to measure the time dependence, with a resolution of several μs, of the temperature at a selected point in the plasma. Alternatively the plate separation can be scanned to measure spatial profiles with time resolution of a few ms.

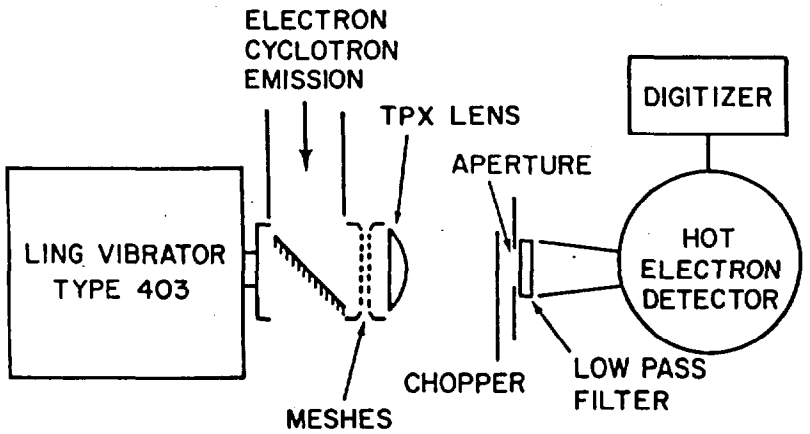

Figure 19: A schematic of an ECE Fabry–Perot system (Costley 1982).

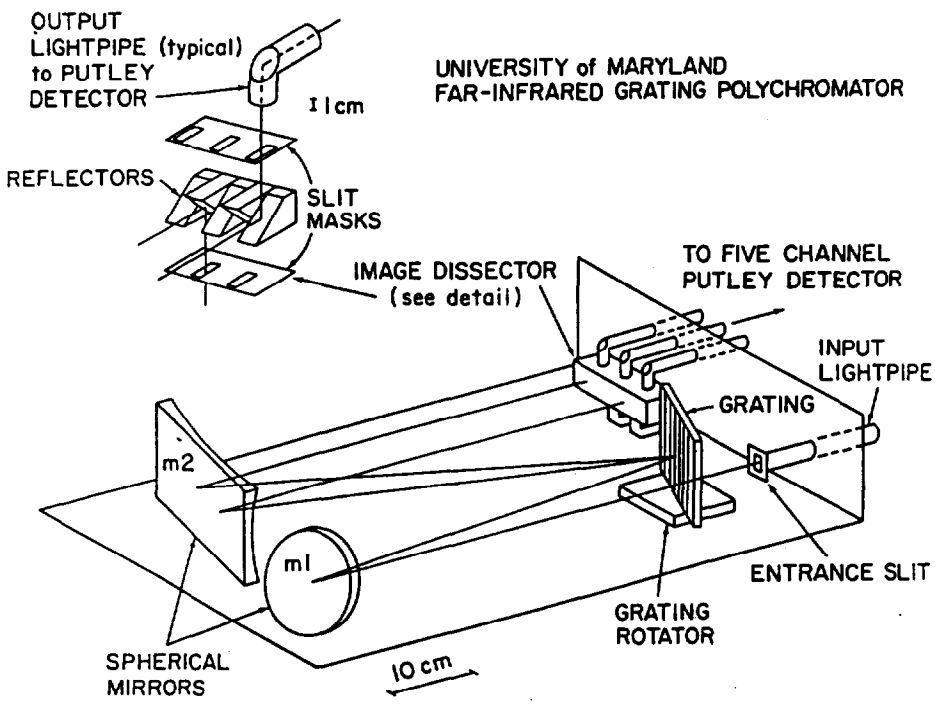

Figure 20: Schematic of a far infrared grating polychromator (Costley 1982)

The temperature at many points in the plasma can be measured simultaneously with good time dependence (typically a few μs) using a *diffraction grating* instrument. A common arrangement has an "echelette" grating mounted in a Czerny-Turner configuration which disperses the radiation into 10 or more detector channels (figure 20). This method is particularly well-suited to measuring the spatial and temporal development of temperature fluctuations.

Very good spatial resolution is obtained using *microwave heterodyne detectors* (figure 21). This method uses well developed microwave techniques. The ECE radiation is mixed with a wave from a local oscillator and the resulting intermediate frequency is amplified and detected. Heterodyne detection has high sensitivity, good frequency resolution and fast response time (1 μs). It has been limited to relatively low frequencies (≤ 150 GHz) in systems using classical microwave techniques but using quasi-optical techniques it may be possible that the range could be extended up to about 500 GHz.

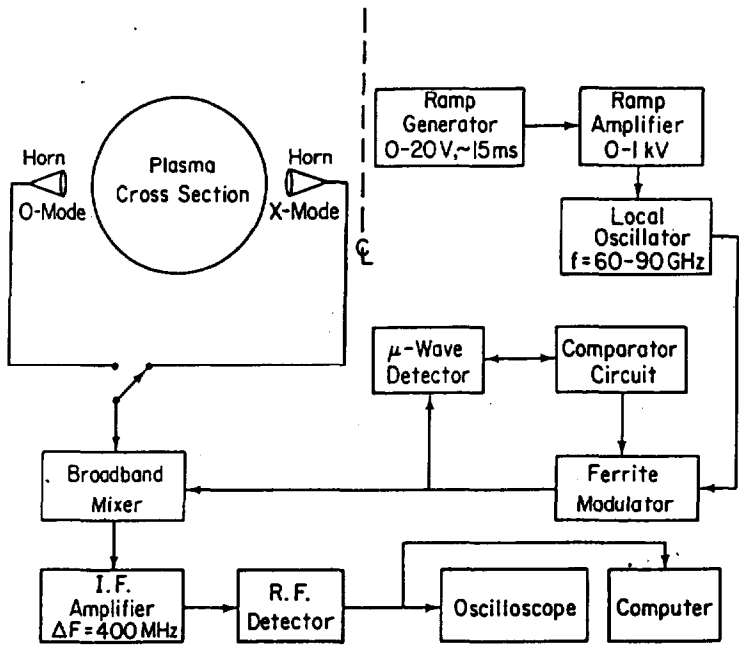

Figure 21: Schematic of ECE super heterodyne system (Costley 1982)

Most tokamak experiments use several of these ECE detection methods in order to take advantage of their different measurement characteristics. The TFTR tokamak has three heterodyne receivers covering the range 75 to 220GHz and a high resolution Michelson instrument which extends the range to 540GHz. JET uses all four methods through an array of antennas that view the plasma along several different chords in the poloidal cross-section. The radiation is transmitted over a distance of about 40 m via oversized microwave wave-guides from the torus to the measuring instruments which are located behind a neutron shielding wall. There are: several Michelson and Fabry-Perot interferometers

which are used for two dimensional spatial profile measurements; a 12 channel grating polychromator which is used for radial profile measurements on a faster time scale; and a 44 channel heterodyne system which is used for measurements with good spatial resolution.

5.2 Electron temperature profile measurements.

Calibration of an ECE system is important because the temperature measurement relies on the intensity of the emission. It is difficult because the temperature of available calibration sources (typically $\leq 10^3$K) is many orders of magnitude less than the plasma temperature (typically $\geq 10^7$K). Reliable calibration techniques have been developed recently which allow the measurement of T_e with a typical absolute accuracy, due to systematic errors, of ±10%. The relative accuracy between different points in the same profile can be as small as ±5%. Comparison between temperatures measured by ECE and by other diagnostic methods (figure 22) has been facilitated by the extensive computerized data bases which exist for many large fusion experiments. The random errors in ECE measurements are much smaller (typically < 1%) than those in Thomson scattering measurements (typically 10%) but the systematic errors are harder to quantify. Careful comparison between the two measurements makes it is possible to determine the magnitude of the systematic errors in the ECE system and has led to a significant reduction in the estimated error.

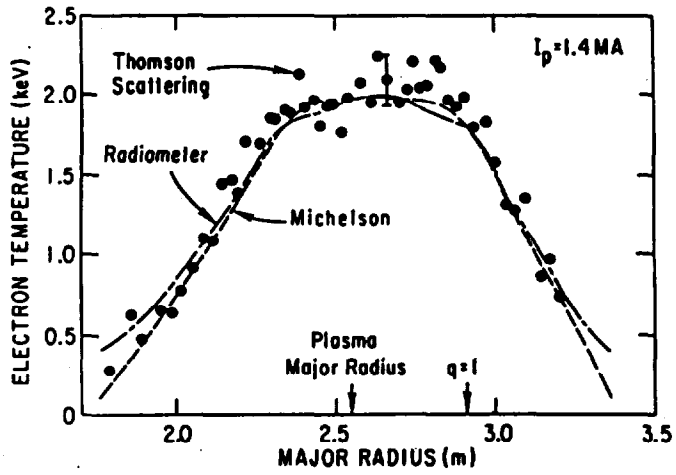

Figure 22: Comparison of independent measurements of the electron temperature profile in JET using Thomson scattering and two ECE methods; radiometer (o−mode fundamental) and Michelson (e−mode second harmonic) (Costley 1986).

5.3 Sawteeth oscillations.

The temperature (and density) in the core of tokamaks fluctuate periodically due to *sawteeth*. This is a widely observed phenomenon and results in periodic loss of energy from the plasma core with a consequential reduction in the

fusion reactivity. Until quite recently, sawteeth appeared to be adequately described by a theoretical model which explained the energy loss phase (usually called the *sawtooth collapse* or *crash*) by a process involving the reconnection of the helical magnetic flux on opposite sides of the surface where $q = 1$ followed by the mixing of the hot core plasma with cooler plasma. Recently detailed studies of sawteeth using improved diagnostics including ECE and soft X-ray emission (a technique which will be described later) have revealed that there are several different types of sawteeth with some features that conflict with the existing model. Various new models are being developed but at the present time there is still no complete agreement between any of the models and all of the experimental data. The detailed structure of the electron temperature during the sawtooth cycle in JET has been studied by Campbell *et al* (1989). The radial temperature profile is measured with good time and spatial resolution ($\approx$ 2 μs and $\approx$ 50 mm respectively) using a 12-channel ECE polychromator viewing the plasma along the equatorial plane. The plasma rotates in the toroidal direction with a frequency of about 2 kHz and sweeps the complete core through the field of view of the ECE diagnostic so that temperature contours in the poloidal plane can be reconstructed from the temperature profiles. The temperature contours in figure 23 were taken immediately after a full sawtooth collapse. A crescent-shaped region of cold plasma has entered the core and the displaced hot plasma has cooled and been

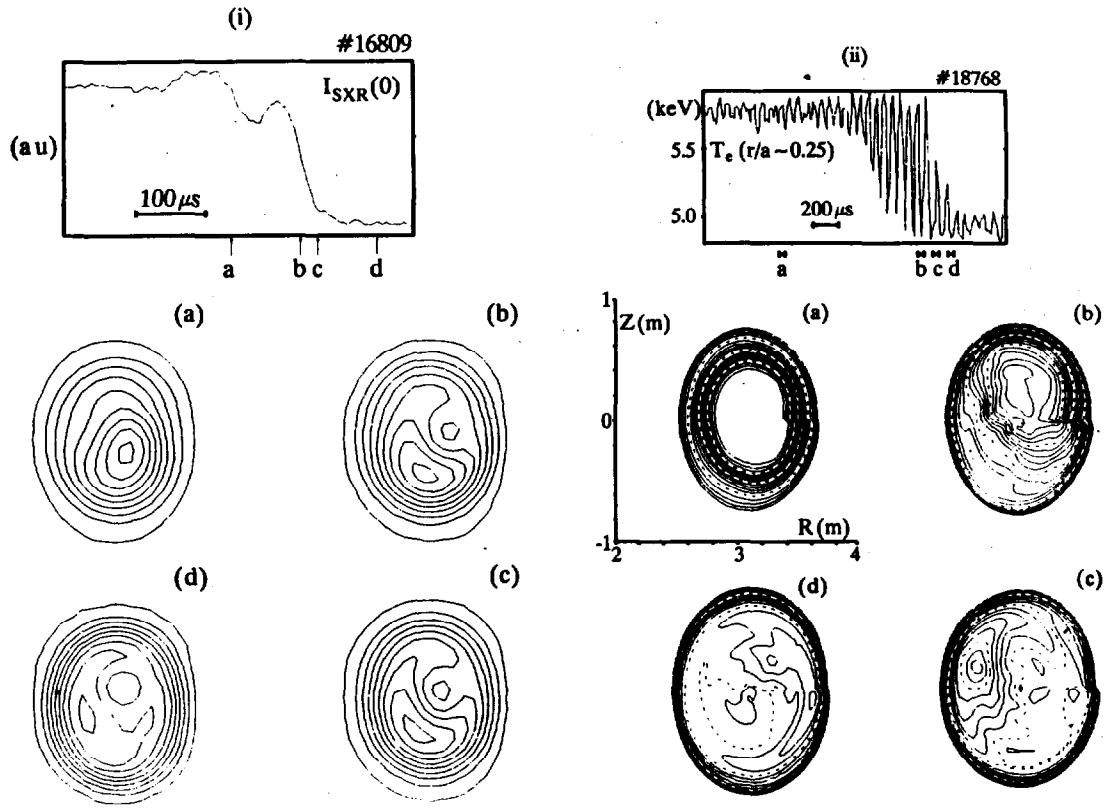

Figure 23: Comparison of sawtooth collapses in JET using (i) soft X-ray emission and (ii) ECE. In both cases there is a characteristic displacement of the hot plasma core into a crescent shaped region.

squeezed into an annular ring. Similar reconstructions of the core plasma can be made with data from X-ray and neutron diagnostics as will be discussed in later sections. High resolution ECE measurements have been used to study the fine structure of temperature profiles and localized flat regions have been observed outside the core. These are identified with the *magnetic islands* that were discussed earlier in the section dealing with magnetic diagnostics.

5.4 Energy and particle confinement

The total kinetic energy in the plasma and the global confinement time can be calculated using temperature profiles measured by ECE and density profiles measured by interferometry or reflectometry. Alternatively both density and temperature profiles can be measured by incoherent Thomson scattering which will be discussed later. Confinement in toroidal magnetic systems is substantially less than would be expected for collisional diffusive processes, even when the so-called *neo–classical* effects due to toroidal geometry are included. Moreover the confinement is further reduced when the heating power is increased. There appears to be a critical value of the temperature gradient which limits the shape of the profile in much the same way that a pile of sand cannot be stacked too high. The cause of the reduced confinement is not understood and remains one of the most important problems in fusion research. There is considerable emphasis on profile measurements and on the determination of the plasma transport coefficients.

The plasma transport coefficients (particle and thermal diffusivity) can be determined experimentally by two main methods. The first method is based on analysis of the steady-state power and particle balances. Analysis of the energy balance requires accurate measurements of the plasma temperature and density profiles. The electron profiles are usually more accurate and readily available than the ion profiles. There are large uncertainties in calculating the power transferred between the ions and electrons and in determining the power deposition profiles. The second method involves perturbing the steady-state profiles either by modulating the heating power or following a sawtooth collapse when the kinetic energy expelled from the plasma core propagates outwards towards the edge, perturbing both the temperature and density. The electron thermal diffusivity can be determined from measurements of the outwardly propagating temperature wave. Callen and Jahns (1977) applied this method using soft X-ray emission to measure the temperature perturbation. Subsequently the technique has been extended using ECE (Tubbing *et al* 1987, Lopez Cardoza *et al* 1988). The grating polychromator and heterodyne systems are capable of simultaneous measurements at different plasma radii.

The values of thermal diffusivity measured by these perturbation methods are usually found to be 2 to 5 times larger than values determined from the power balance. A full analysis of the transport of perturbations (Gentle 1988, de Haas *et al* 1991) shows that the coefficients can be different from the equilibrium values. Moreover density and temperature perturbations are coupled because density and temperature fluxes appear in the energy transport equation and because the transport coefficients themselves may depend on the density, temperature and their gradients. It is necessary to measure simultaneously both the density and temperature perturbations in order to determine the thermal and particle transport coefficients. Density perturbations have been measured in TEXT (Kim *et al* 1988, Brower *et al* 1990) using multi-chord interferometry and in JET (Sips *et al* 1991) using reflectometry. The particle diffusivity measured in JET by these techniques is substantially smaller than the thermal diffusivity. It must be stressed that the steady–state coefficients may have different values. A serious conflict in fusion research is that improving the energy confinement also leads to improved particle confinement which will be undesirable if it leads to accumulation in the plasma of helium from alpha particles or impurities released from the wall.

6. Photon scattering

6.1 Incoherent Thomson Scattering

Incoherent Thomson scattering is used to measure plasma temperatures and densities (Evans and Katzenstein 1969, Shefield 1975). This technique has held a special place in the history of fusion diagnostics since it was used by a joint British and Russian team to measure the electron temperature in the T3 tokamak at the Kurchatov Institute in Moscow. These results (Peacock *et al* 1968), which confirmed earlier measurements by less reliable methods, showed that tokamaks were much hotter than pinches and stimulated the rapid development of tokamaks outside the USSR. The method is based on the elastic scattering of photons from the plasma electrons (Nielsen 1982, Salzmann 1986, Gusev 1986, Gowers 1991). The scattering from individual electrons is incoherent so that collective effects can be ignored when $\alpha = \lambda/(4\pi\lambda_D \sin \theta/2) < 1$ (where λ is the wavelength of the scattered light in the plasma, $\lambda_D = (kT_e/4\pi n_e e^2)^{0.5}$ is the Debye length and θ is the scattering angle between the directions of propagation of the incident and scattered photons). The spectrum of the scattered photons gives the one-dimensional electron velocity distribution function (parallel to the direction that is normal to the bisector of the angle θ) and thus the electron temperature, whilst the total number of scattered photons gives the electron density.

6.1.1. Laser sources. The Thomson scattering cross-section is very small ($\approx 6.6\times10^{-29}$ m^2) and consequently only a small fraction ($\approx 10^{-10}$) of the incident photons is scattered at typical plasma densities ($\approx 10^{20}$ m^{-3}). In order for the scattered signal to be larger than other light emitted by the plasma (principally bremsstrahlung and impurity line radiation) the source must be a high power Q-switched laser. The most commonly used sources are ruby ($\lambda = 0.6943\mu$m) and neodymium ($\lambda = 1.06$ μm in the fundamental or 0.53 μm if frequency-doubled) lasers. These wavelengths are in a region of the spectrum where plasma emission is relatively weak and where there are sensitive, low-noise detectors. Laser pulse energies in the range 1 to 20 J are required. The repetition rate for ruby lasers is limited (typically to less than a few Hz) due to thermal effects but higher repetition rates (up to about 100 Hz when yttrium aluminium garnet (YAG) is used as the laser medium) can be obtained with neodymium lasers.

The spectrum of the scattered light is broadened by the Doppler effect. In high-temperature plasmas it is also shifted by relativistic effects towards the blue end of the spectrum. For a plasma temperature of 10 keV the scattered spectrum at $\theta \approx 90^0$ with a ruby laser source lies in the range 0.35 to 0.95 μm. The scattered light is spectrally analyzed in various ways, including diffraction gratings, prism spectrometers and interference filters. If the electron distribution is assumed to be a Maxwellian, the temperature can be determined from the ratio of intensities at two suitable wavelengths. However in most experiments the spectrum is measured at several wavelengths (typically up to 10) in order to determine the complete (one-dimensional) electron velocity distribution function. A major advantage of Thomson scattering for temperature measurements is that it does not need to be absolutely calibrated; calibration of the relative sensitivity of the different channels is sufficient. Absolute calibration is required for density measurements and is usually done either by Rayleigh scattering from neutral gas in the torus or by cross-calibration with a density interferometer.

6.1.2. Spatial profile measurements. To measure the temperature and density at a single point in the plasma, the incident laser light is focused onto a small volume with dimensions of the order 10^{-3} m. In order to measure profiles with this arrangement it is necessary to make measurements at different spatial points in successive plasmas but this is obviously tedious and relies on good plasma reproducibility. A particular advantage of spatial-scan Thomson scattering systems is that the electron temperature and density are measured simultaneously in space and time. Several methods have been developed to measure the full spatial profile during a single laser pulse. One approach is

to replicate the scattered light collection and analyzing systems with separate systems viewing a different point along the plasma chord that is illuminated by the laser. The system used in the TFR tokamak about a decade ago had 8 separate collection systems (LaSalle and Platz 1979). Systems constructed more recently have many more spatial channels; for example the DIII-D Thomson scattering system has 40 spatial channels and a high repetition rate is achieved by multiplexing eight 20 Hz Nd:YAG lasers. An alternative arrangement is the "TV Thomson scattering system" developed on the PLT and PDX experiments (Bretz *et al* 1978) and more recently applied to the TFTR experiment (Johnson *et al* 1985). The scattered light is collected by a wide-angle lens which images the whole illuminated chord of plasma via a linear array of optical fibres onto the entrance slit of a diffraction grating spectrometer. The dispersed light is amplified with a micro-channel plate intensifier which is coupled to a cooled silicon target vidicon. This system gives a two-dimensional readout where one axis corresponds to wavelength and the other to spatial position. Typical profiles are shown in figure 24.

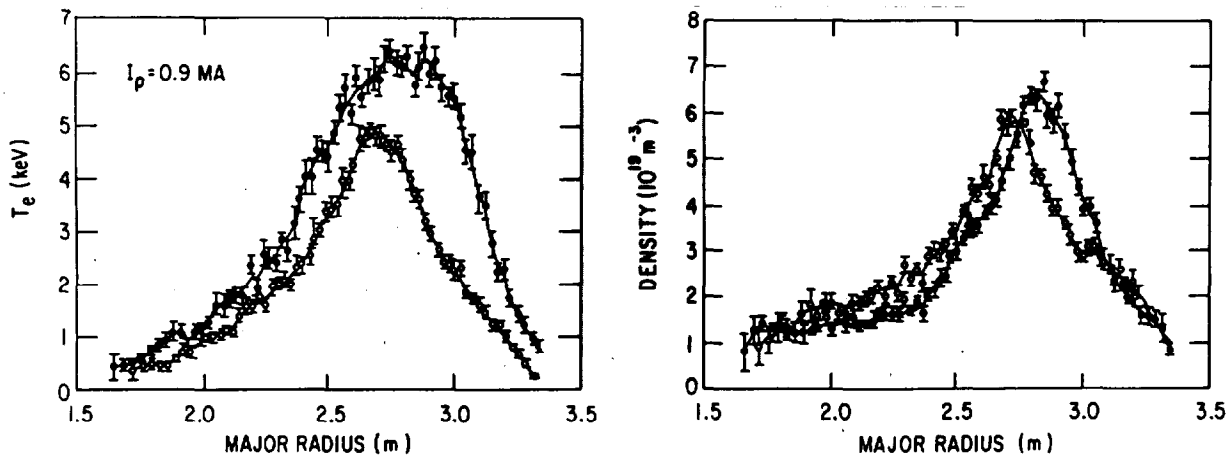

Figure 24: Typical profiles of electron density and temperature in TFTR measured with Thomson scattering. The solid points are for a "super shot" plasma which had improved fusion performance (Hawryluk et al 1987)

A novel spatial-scan diagnostic suitable for large fusion experiments has been developed on JET (Salzmann *et al* 1988). This is based on laser ranging principles (LIDAR) and uses a ruby laser pulse whose duration is much shorter than the transit time of the laser light across the plasma so that the time of arrival of light at the detector can be related to spatial position. The back-scattered light is collected and spectrally analyzed using interference filters and very fast photo-multiplier detectors to determine the electron temperature and density profiles The spatial resolution, which is determined by the duration of the laser pulse (300ps) and by the time resolution of the detector (also about 300ps), is typically 0.08m. Faster detectors based on streak camera principles together with lasers with shorter pulse durations and faster repetition rates are being developed to further improve the

performance. The LIDAR technique requires only a single line-of-sight access to the plasma and is therefore particularly well-suited to the next generation of fusion experiments where access will be severely limited by structural components (Mukhovatov *et al* 1991).

6.1.3. Measurement of q(r). If the electrons are in a magnetic field, the scattered light spectrum is modulated at the electron cyclotron frequency when the magnetic field vector is parallel to the direction that bisects the scattering angle θ. This effect has been used to measure the internal poloidal magnetic field and the safety factor $q(r)$, quantities which are of considerable interest for tokamak stability. In a hot plasma the scattered photons are spread through a large number of harmonics (> 100) and the intensity in a single harmonic is too low to be detectable. Measurements have been made on the DITE tokamak by Forrest *et al* (1978) with an elegant multiplexing technique which uses a Fabry-Perot interferometer whose free spectral range is set equal to the cyclotron frequency allowing all the harmonics to pass when the angular condition is satisfied. This determines the direction of the total field **B** from which the poloidal field component can be derived since the toroidal field component is known. This elegant method is difficult and consequently it has not been applied widely.

6.2 Collective Thomson Scattering

Collective Thomson scattering refers to the process where the electromagnetic wave interacts with electrons on a scale length longer than the Debye length. There are two main applications: (i) light scattered from the cloud of electrons surrounding each ion is used to measure the energy distribution and temperature of the ions; (ii) light scattered from waves and fluctuations is used to study plasma density perturbations. Interpretation of the coherent scattered spectrum is more ambiguous than for the incoherent case. Distortions can be caused by impurity (ie. non-hydrogenic) ions, which will have similar temperatures but lower thermal velocities due to their heavier masses.

6.2.1. Ion temperature measurements. The prospect of a reliable ion temperature diagnostic has motivated considerable efforts to develop the collective scattering method, but progress has been slow due to the difficulty of finding a suitable high-power laser source. The condition ($\alpha = \lambda/(4\pi\lambda_D \sin\theta/2) > 1$), requires longer wavelengths for collective scattering than for incoherent scattering ($\lambda_D \approx 75$ μm for $T_e \approx 1$ keV and $n_e \approx 10^{19}$ m^{-3}). Infra-red lasers (for example CO_2 lasers with $\lambda = 10.6$ μm) have sufficient power, but the condition $\alpha > 1$ requires extremely small

scattering angles ($\theta < 1^0$). This gives difficulties with spatial resolution and with excluding incident radiation from the detector. A laser source in the far infra-red is required for scattering angles that are large enough to permit good spatial resolution in tokamaks. The optically-pumped D_2O laser has a stimulated Raman transition at 385 μm and Schottky barrier diodes mixers allow heterodyne detection at this wavelength with good sensitivity and bandwidth. The first results from collective Thomson scattering using a pulsed D_2O laser were reported by Woskoboinikov *et al* (1983) but the ion temperature could not be measured due to problems with stray light. Recent improvements in laser and detector technology have led to successful measurements of ion temperature in the TCA tokamak (Behn *et al* 1989, Siegrist 1991). A schematic of the TCA diagnostic system is shown in figure 25. A high power CO_2 laser delivers 600 J in a single 1.4 μs single mode pulse into the D_2O resonator which produces 0.5 J at 385 μm.

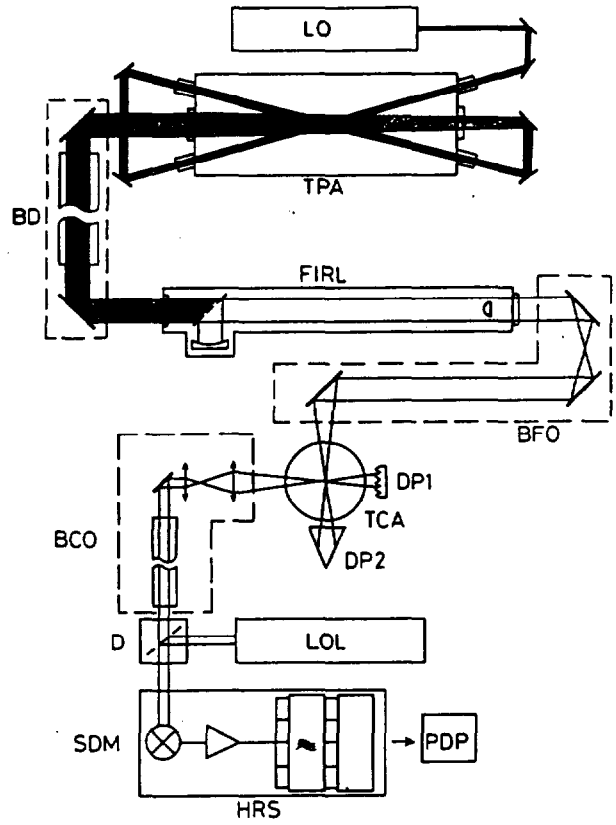

Figure 25: Configuration of the collective scattering system on the TCA tokamak (Siegrist et al 1991).

6.2.2. Fast ion distributions. Collective scattering also has important applications in the measurement of fast-ion, especially the alpha particle, distributions. Because far infra-red sources are too weak, proposals for alpha particle diagnostics have concentrated on small angle ($\theta \approx 1^0$) scattering at 10 μm using CO_2 lasers or at larger angles ($\theta > 30^0$) and longer wavelengths ($\lambda \approx 2$ mm) using powerful microwave sources. This wavelength is chosen because the plasma background light (principally electron cyclotron emission) is low and there are suitable gyrotron sources and detectors. These diagnostic techniques are being developed in the JET and TFTR experiments.

6.2.3. Fluctuations. Collective scattering is also sensitive to macroscopic, non-thermal density fluctuations. These may be caused by various types of plasma waves including naturally occurring instabilities as well as those deliberately launched to heat the plasma. There has been considerable interest in using collective scattering to study density fluctuations as a possible cause of enhanced plasma transport. For scattering from a density perturbation with wavelength λ_n, the scattered radiation has to satisfy both the Bragg condition $\vartheta = 2\sin^{-1}(\lambda/\lambda_n)$ and the condition $\alpha = \lambda/(4\pi\lambda_D \sin \vartheta/2) > 1$ for collective scattering. Far infra-red and millimeter-wave radiation gives a good compromise between the various criteria (Luhmann *et al* 1991). Experiments have been carried out in the TEXT, DII-D, JIPPT-IIU, ASDEX and several other tokamaks. Infra-red scattering using CO_2 radiation ($\lambda = 10.6$ μm) results in smaller scattering angles so that the scattered radiation remains within the divergence angle of the unscattered beam. The two beams can be mixed to form a homodyne detection system (Slusher and Surko 1980).

7. Photon Emission

7.1 Emission spectroscopy

Plasma spectroscopy owes much of its early development to the study of astrophysical plasmas. The radiation emitted by a plasma conveys information about the properties of the immediate plasma environment as well as those of the emitting ion. Many plasma properties including electron temperatures and densities can be measured by spectroscopy, though the most extensive applications in fusion research are to study impurities (de Michelis 1986) and to measure ion temperatures. Magnetically-confined plasmas contain small amounts of impurity ions in addition to the main hydrogenic ions. These impurities have various deleterious effects on the plasma characteristics, including diluting the fusion fuel and cooling the plasma by radiation. Incoming impurity atoms are excited and ionized by electron impacts and, since the electron temperature profile is centrally peaked, impurities are ionized to progressively higher charge states as they penetrate into the plasma (figure 26). In a steady-state situation the inward flux of impurities is balanced by outward diffusion so that the radius of the maximum concentration of each ionization state is determined by the electron temperature and by the transport rates. The impurities are conveniently categorized by their atomic charge Z. Low-Z impurities, such as carbon and oxygen, may be present at concentrations of several percent of the electron density and are usually fully-ionized in the hot plasma core. Medium-Z impurities, such as nickel, iron and chromium, which are typical wall materials, are usually present in

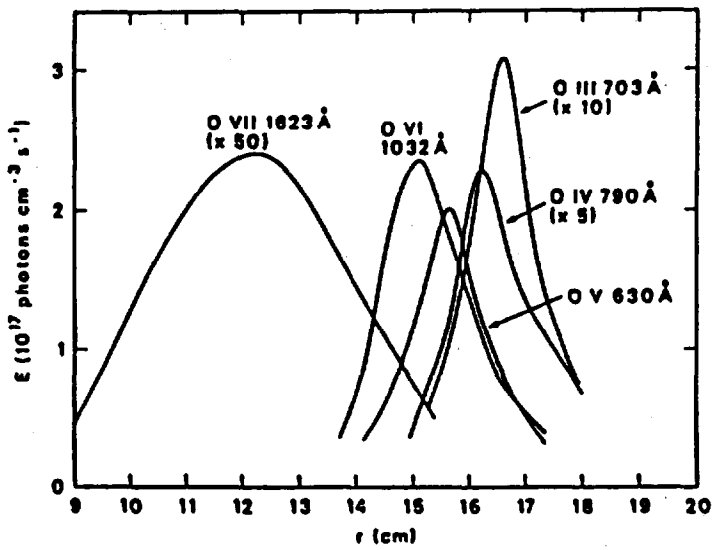

Figure 26: Spatial profiles of oxygen spectral lines in TFR (de Michelis 1986)

much smaller concentrations. They are only partly-ionized in small and medium sized plasmas but are found in the hydrogen- and helium-like states in the cores of the largest tokamaks. High-Z impurities, such as molybdenum and tungsten, are particularly damaging as they remain incompletely ionized throughout the plasma. Small concentrations of high-Z impurities cause significant cooling of the core and would make ignition impossible if present in a fusion reactor.

The most intense impurity emission lines are those having ground state configurations with either one or two *s*-electrons with the emission concentrated in the $ns-np$ transitions. Ionization states with complex structures are in general more difficult to detect since they emit weak lines and they are more difficult to interpret in terms of absolute impurity concentrations. Several steps are required to deduce impurity concentrations from the measured line intensities. First a suitable line for each ionization state is selected and its intensity is measured along different chordal lines-of-sight. These data are Abel-inverted to obtain the emissivity profiles; in non-circular plasmas this requires knowledge of the magnetic flux surfaces. Then the corresponding ion densities are calculated using values of the branching ratios and rate coefficients derived from atomic physics. This procedure is repeated for each ionization state in order to determine the total concentration of each important impurity. Thus a complete study of impurity concentrations requires extensive spatially-resolved measurements. A common short cut is to limit the measurements to a few strong emission lines of representative ionization states and to use an impurity transport model to estimate the impurity concentrations.

7.1.1. The ultra–violet spectrum. Many of the most important emission lines are in the ultra-violet and for many years effort was concentrated in this region. Grating spectrometers are widely used in a variety of different configurations (figure 27) including plate instruments for spectral surveys and instruments with photo-multipliers for time-resolved measurements of selected lines. Instruments with channel plate detectors have been developed to combine both functions. Vacuum instruments are required for wavelengths shorter than about 200 nm (about 120 nm using magnesium fluoride windows). Diffraction gratings must be used at grazing incidence angles for wavelengths shorter than 30 nm. Reflecting surfaces and light relay systems are inefficient at shorter wavelengths so that the instruments have to be close to the plasma where their sensitive detectors are in direct line-of-sight. This leads to difficulties with interference from background light and from neutrons and gamma radiation.

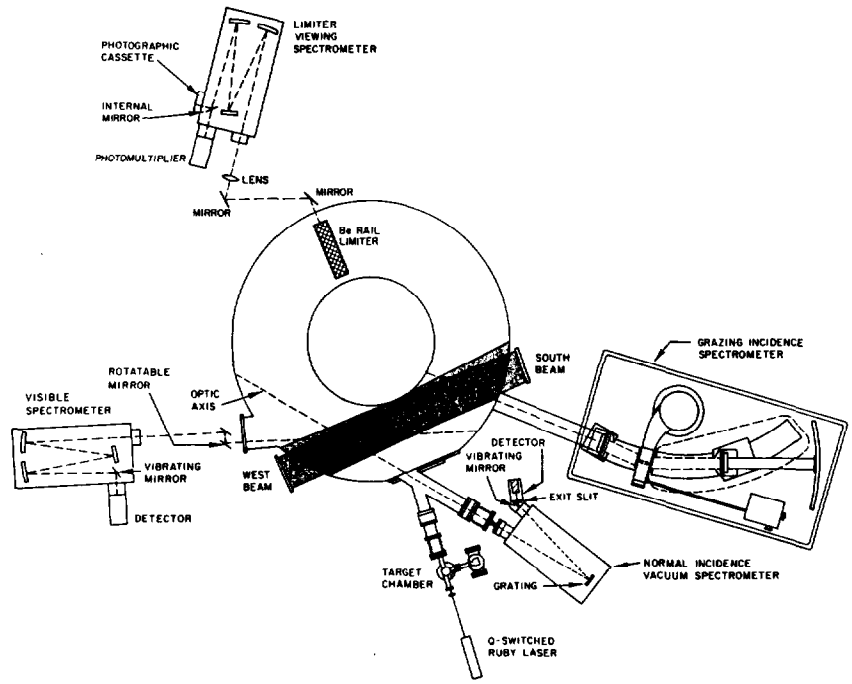

Figure 27: Arrangement of spectrometers on ISX–B showing the range of instruments used on a typical fusion experiment (Isler 1992).

7.1.2 The visible spectrum. The operational difficulties with ultra-violet spectrometers in high-radiation backgrounds has stimulated the development of spectrometers that can be placed remote from the plasma. An obvious solution is visible-light spectroscopy. Visible light is easily routed to a remote instrument by relay optics or fibres. Spectral lines are isolated by interference filters or monochromators. Measurements in visible light are particularly well-suited to diagnosing the plasma edge. Recent theoretical work has provided a reliable basis for the interpretation of visible spectra where the transitions are in general between complex states. The effective ion charge $Z_{eff} = \sum Z_i^2 n_i / n_e$ (where the summation is taken over all charge states

of all impurity species) can be calculated in principle from the measured impurity concentrations but it is more easily and reliably measured from the enhancement of the bremsstrahlung continuum in a region of the spectrum where there are no strong emission lines. This is most conveniently done in the visible. The Z_{eff} profile can be measured with a suitable array of photo-diodes or photo-multipliers.

7.1.3 The soft X-ray spectrum. The X-ray spectrum emitted by a hot, magnetically-confined plasma consists of line emission from excited impurity ions superimposed on a continuum of bremsstrahlung from the free electrons. X-ray diagnostics are used to measure a variety of plasma quantities and there have been many developments during the last decade (Hill 1986). The bremsstrahlung from free-free and free-bound transitions has a strong dependence on the electron temperature and was one of the earliest plasma diagnostic methods. The bremsstrahlung spectrum is usually measured using a pulse-height analysis system based on a cooled, lithium-drifted silicon detector. This is essentially a P.I.N. diode with a large volume of intrinsic silicon. When a X-ray photon is absorbed, it produces a number of electron-hole pairs proportional to the photon energy. The detector output pulses are sorted electronically to give the photon energy spectrum. Sometimes interpretation is complicated by the presence of impurity emission lines which distort the bremsstrahlung spectrum. The time resolution is limited by the counting rate and by the need to accumulate sufficient counts to resolve the spectrum. Because of these limitations, the pulse-height analysis method has been superseded to a large extent by Thomson scattering and electron cyclotron emission as a diagnostic for electron temperature measurements in tokamaks but it is still used extensively in pinches and other high-density fusion experiments. In tokamaks, X-ray pulse-height systems are useful for studies of impurities and transport; for example a six-channel system is used in TFTR to measure the time dependence of Z_{eff} and concentrations of metal impurities.

Many of the strongest resonant emission lines are in the soft X-ray region (for example helium-like Ni XXVII at 1.58Å) which is consequently an important area for measurements. Plane crystal spectrometers are used for spectral line identification and intensity measurements. The higher resolution of curved crystal instruments is particularly well-suited for line broadening measurements of ion temperatures and macroscopic rotational velocities. Remote measurement methods have also been developed using X-ray crystal spectrometers where the crystals are used both to disperse the light and as the reflecting elements in a relay system that transports the X-rays to detectors located outside the radiation shielding (figure 28).

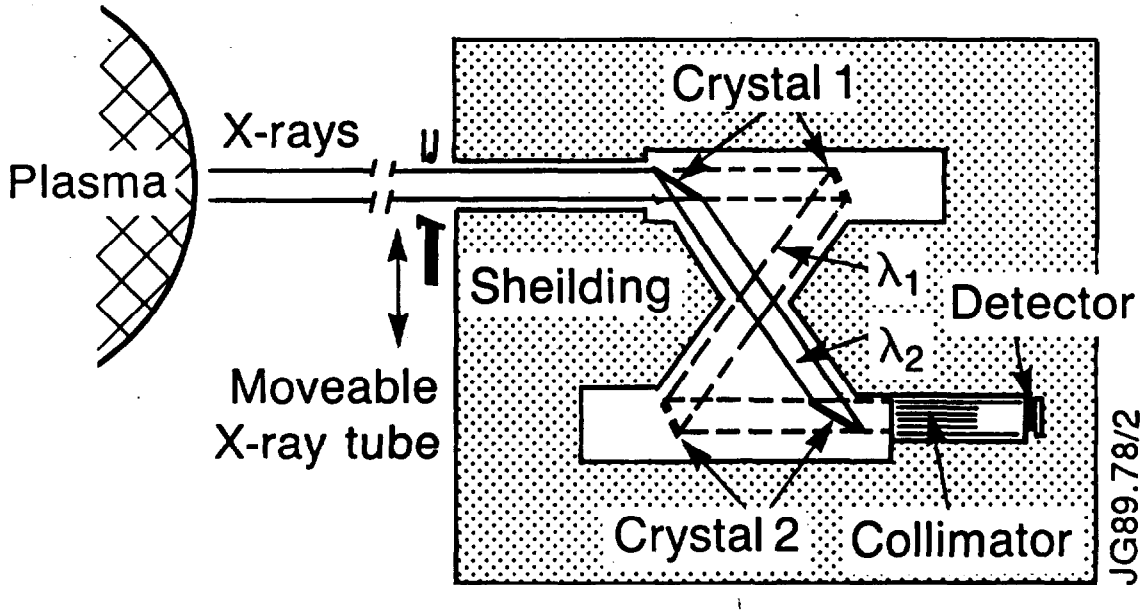

Figure 28: Schematic of the radiation–shielded, double–crystal X–ray monochromator developed for JET.

7.1.4 Ion temperatures and macroscopic velocities. Plasma ion temperatures and macroscopic rotational velocities can be determined from the Doppler broadening and shifting of impurity emission lines. There is usually strong energy coupling between the impurity and hydrogenic ions so that the temperatures and velocities measured for the impurity ions are representative of the hydrogenic ions. Typical tokamak conditions require a spectral resolution of order $\lambda/\Delta\lambda \geq 10^4$. High-resolution, normal-incidence grating spectrometers are used in the visible and near ultra-violet regions of the spectrum to measure low-Z impurity lines emitted from near the plasma edge. High-resolution X-ray crystal spectrometers are used to observe lines emitted by highly-ionized states of high-Z impurities in the plasma core.

7.3 Bolometers

Although the total power lost from the plasma by impurity radiation can be calculated in principle by summing the losses for each impurity type and ionization state, this would be very tedious and imprecise. The total radiated power is usually measured with bolometers which have a flat response over a wide spectral range in the ultra-violet and soft X-ray regions which contain

most of the strong emission lines. Several different types of bolometer have been developed (Stott 1982b, Ochando 1991) including pyroelectric devices, thermopiles, and resistance bolometers. Some of these are easily damaged by neutrons and are not suitable for experiments with high radiation environments. Metal resistance bolometers consist of a thin plastic foil with a thin gold or platinum absorber layer on the side facing the plasma and a gold resistor labyrinth on the reverse side. The temperature rise of the bolometer is determined by the change in resistance which is measured using an electronic bridge circuit. Abel-inverted profiles of the radiated power density are measured using arrays of bolometers viewing the plasma through suitable collimating apertures. For most conditions of tokamak operation, the radiated power density profiles are poloidally symmetric. However there are some conditions when asymmetric bright spots appear, indicating a thermal instability which can evolve into plasma detachment from the limiter (figure 29).

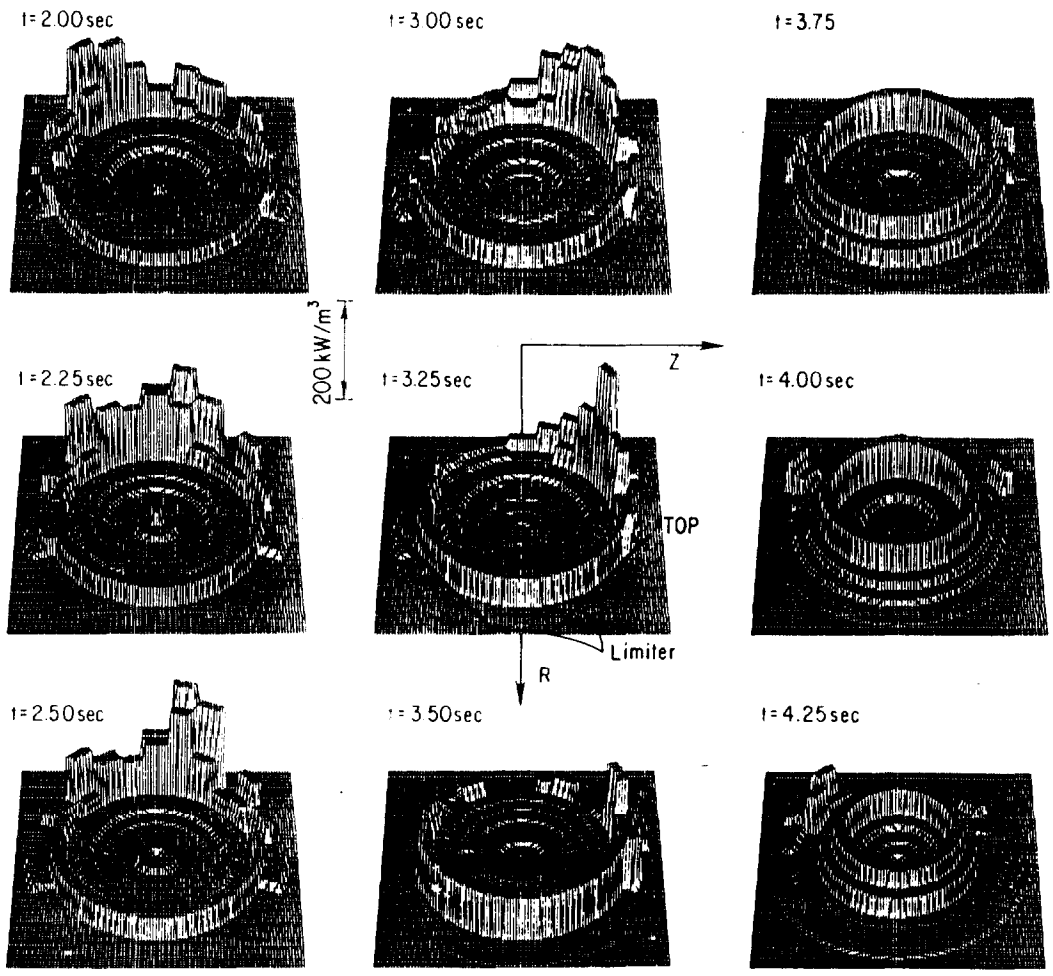

Figure 29: Tomographic reconstructions of radiated power density in TFTR showing the development of a localized region of high radiation (a "MARFE") and the subsequent detachment of the plasma from the limiter (Schivell 1987).

A major limitation with passive emission spectroscopy is that low-Z impurities in the plasma core are fully ionized and consequently do not emit. These ions can be transformed into lower ionization states by charge-exchange reactions with neutral hydrogen atoms

$$H^0 + A^{+q} \Rightarrow H^+ + A^{+(q-1)}.$$

The charge-exchange reaction leaves the ion in an excited state and is followed by prompt radiative decay emitting a spectral line (figure 30) whose intensity allows the determination of the density of the parent, fully-ionized impurity ion. Spectral line emission by the charge-exchange process in fusion plasmas was first observed in the ORMAK and T-4 tokamaks in the late 1970's. Since then it has been developed into a powerful diagnostic for impurity densities, ion temperatures and plasma rotation velocities that is now applied on many fusion experiments (Isler 1987 and 1991).

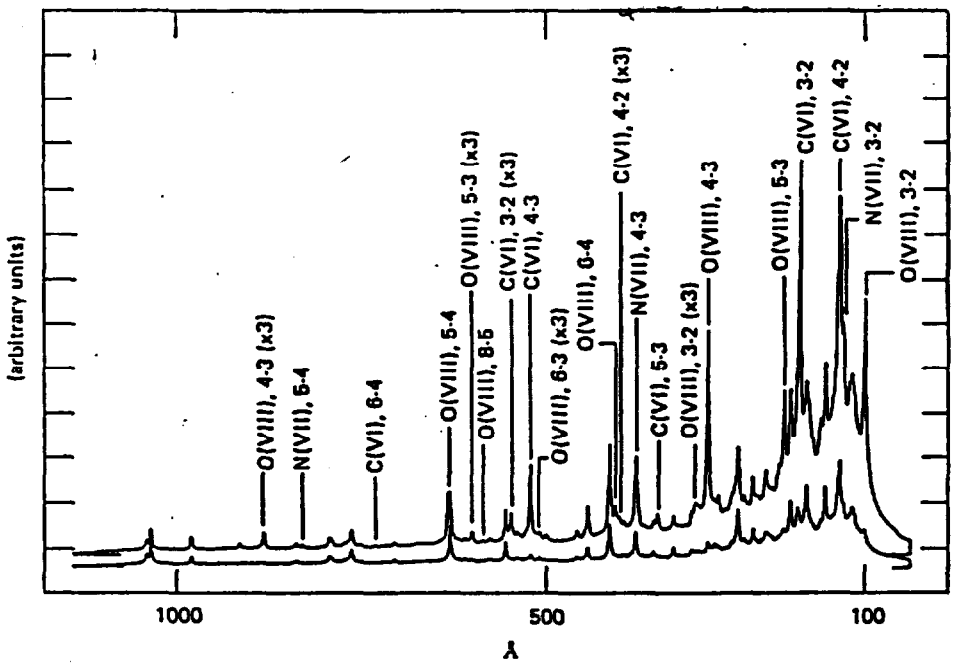

Figure 30: Enhancement of spectral line intensities in ASDEX with neutral beam injection (upper trace) compared to passive emission (lower trace). Note the enhancement of the emission from fully ionized states O(VIII) and C(VI).

In most applications the source of hydrogenic atoms is an injected neutral beam. Energies up to about 100 keV and currents of several Amperes are required to penetrate to the plasma core. Suitable neutral beams have been extensively developed for heating fusion plasmas. In some applications charge-exchange spectroscopy makes use of the heating beams (figure 27); in others there is a dedicated "diagnostic" neutral beam (figure #31). The measurements are localized to the region where the neutral beam and the line-of-sight of the spectrometer intersect. Good spatial and temporal resolution

is achievable with suitable sight-lines. Spatial profiles are measured by scanning the direction of either the neutral beam or the spectrometer.

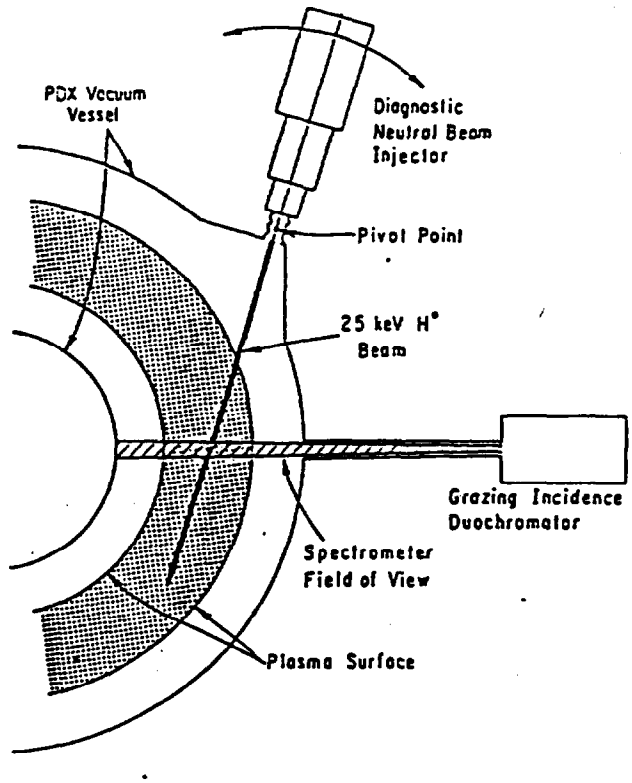

Figure 31: Schematic of the charge–exchange spectroscopy diagnostic on PDX. Radial profiles of fully–ionized carbon and oxygen impurities have been measured by scanning the diagnostic neutral beam.

Charge-exchange spectroscopy is used widely for the measurement of the densities of fully-ionized low-Z ions, particularly carbon, oxygen and nitrogen. A recent application has been to the study of helium transport which is important for predicting the exhaust of alpha particles in a fusion reactor. As already noted, these ions are fully ionized and thus cannot be detected directly by passive emission spectroscopy. For quantitative measurements of ion densities, it is necessary to know the effective charge-exchange cross-sections and the rates at which each excited state is populated by cascades from higher states. The application of charge-exchange spectroscopy to fusion plasmas has stimulated intensive theoretical calculations and experimental measurements of the necessary cross-sections. This work has improved considerably the accuracy of interpreting spectroscopic data.

The charge-exchange process populates highly-excited states which emit spectral lines at wavelengths that are long enough for accurate measurements of ion temperatures from the Doppler line broadening and plasma rotation velocities from the line shift. The technique has been applied over a remarkably wide range of temperatures; from 100 eV in the CHS torsatron experiemnt to 20 keV in the JET tokamak (figure 32).

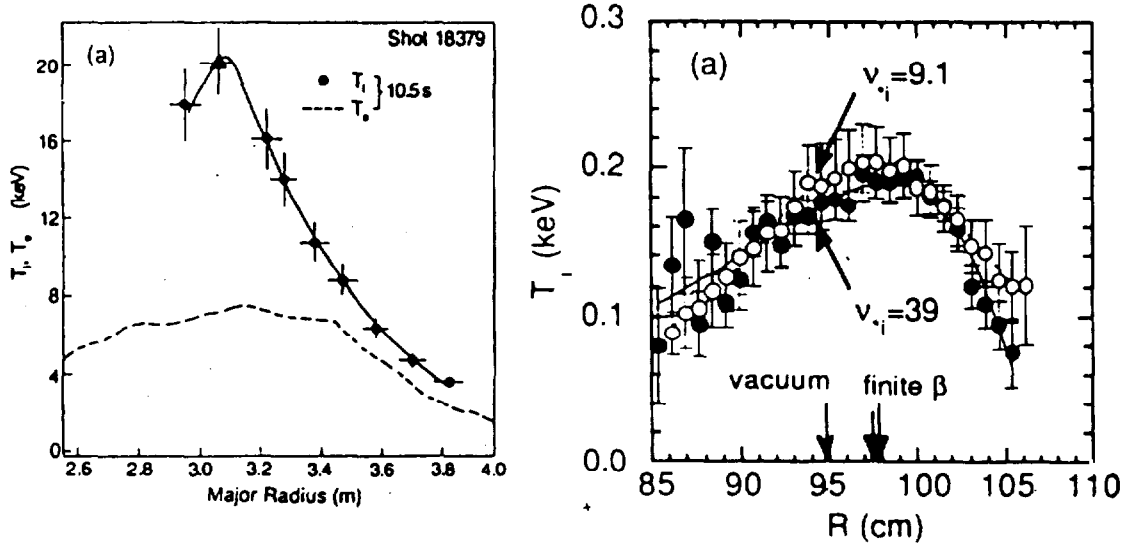

Figure 32: Ion temperature profiles measured by charge–exchange spectroscopy of the 529.2 nm line of C^{5+} in the CHS torsatron (Ida et al 1991) and the JET tokamak (Weisen et al 1989). Note the wide range of temperatures from 0.1 keV in CHS to 20 keV in JET

7.5 Laser–induced fluorescence

Laser-induced fluorescence is a spectroscopic technique based on the selective excitation of specific atomic transitions by absorption of resonance radiation from a suitable laser (Muraoka and Maeda 1991). The selective excitation causes an intensification of the spontaneous emission. The interpretation is simplified by arranging that the laser is sufficiently powerful to saturate the pumped transition. This technique is particularly suitable for measurements of hydrogen, deuterium and impurity atoms or impurity ions in low-ionization states. The spectral range from about 1000 nm down to about 300 nm is covered by tunable dye lasers with a wide range of organic dyes and pumped by flash lamps or by excimer or Nd:YAG lasers. Frequency doubling and tripling techniques are used to extend the range to shorter wavelengths in the vacuum ultra-violet.

Temporally and spatially resolved measurements of the density and velocity of high-Z impurities have been made in some tokamaks but this technique has not yet been universally applied. The measurement of neutral hydrogen densities is an important application of laser fluorescence. Ideally this would be done by exciting the Lyman α transition (λ = 121.6 nm) but ultra-violet laser sources have insufficient power and tunability despite intensive development efforts over the past decade. Measurements have been made using the Balmer α (λ = 656.3 nm) transition, but this does not give the ground-state density.

7.6 Low–Z atomic beams

Atomic beam techniques have been developed for measuring edge density and temperature profiles (Kadota *et al* 1982). Electron density profiles are determined by measuring the attenuation of a neutral beam of a suitable species like sodium or lithium for which the ratio of the ionization and excitation rates is only weakly dependant on the temperature. Electron temperature profiles are determined using a beam of carbon or helium for which the ionization rate has a strong dependence on electron temperature. Low energy beams capable of penetrating a few cms into a typical edge plasma are produced using thermal oven or laser ablation sources. Higher energy beams capable of deeper penetration are produced by accelerating an ion beam and neutralizing it by charge-exchange. The beam intensity is measured through a suitable spectral emission line using filters and silicon diode arrays or photo-multipliers. Spatial localization with a typical resolution about 1mm is obtained by imaging the beam onto an array of detectors.

Lithium beam techniques have been used for poloidal field measurements in the Pulsator (McCormick *et al* 1977) and ASDEX tokamaks (McCormick 1986). The resonance line emitted by transitions between the first excited and the ground states is a Zeeman triplet. The pitch-angle of the tokamak magnetic field is determined from the plane of polarization of the central component of the triplet which is isolated by means of a Fabry-Perot interferometer. In the ASDEX experiments, the safety factor in the plasma core is observed to rise above unity when sawteeth are suppressed by lower hybrid current drive (McCormick *et al* 1987). A fundamental problem with lithium beam methods is the difficulty of penetrating a large, dense plasma. High-speed lithium pellets that can penetrate deeper than beams are being developed to determine q-profiles in ALCATOR and TFTR (Terry *et al* 1990). Two methods are being tested: one is based on observing the angle of polarization of the emitted light; the second is based on the shape of the emitting lithium cloud.

An ingenious combination of the lithium beam technique with laser-induced fluorescence is used to measure the plasma current density in the TEXT tokamak (figure 33). A dye laser is directed along a major radius collinear with a 95 keV lithium neutral beam. The laser is tuned to match the central π component, but not the shifted σ components, of the LiI resonance line at 670.8 nm. The plane of polarization of the laser is rotated at 50 kHz. The π component is excited only when the plane of polarization is parallel to the local magnetic field. The direction of the local magnetic field is determined from the phase of the fluorescence signal relative to the laser (West 1986).

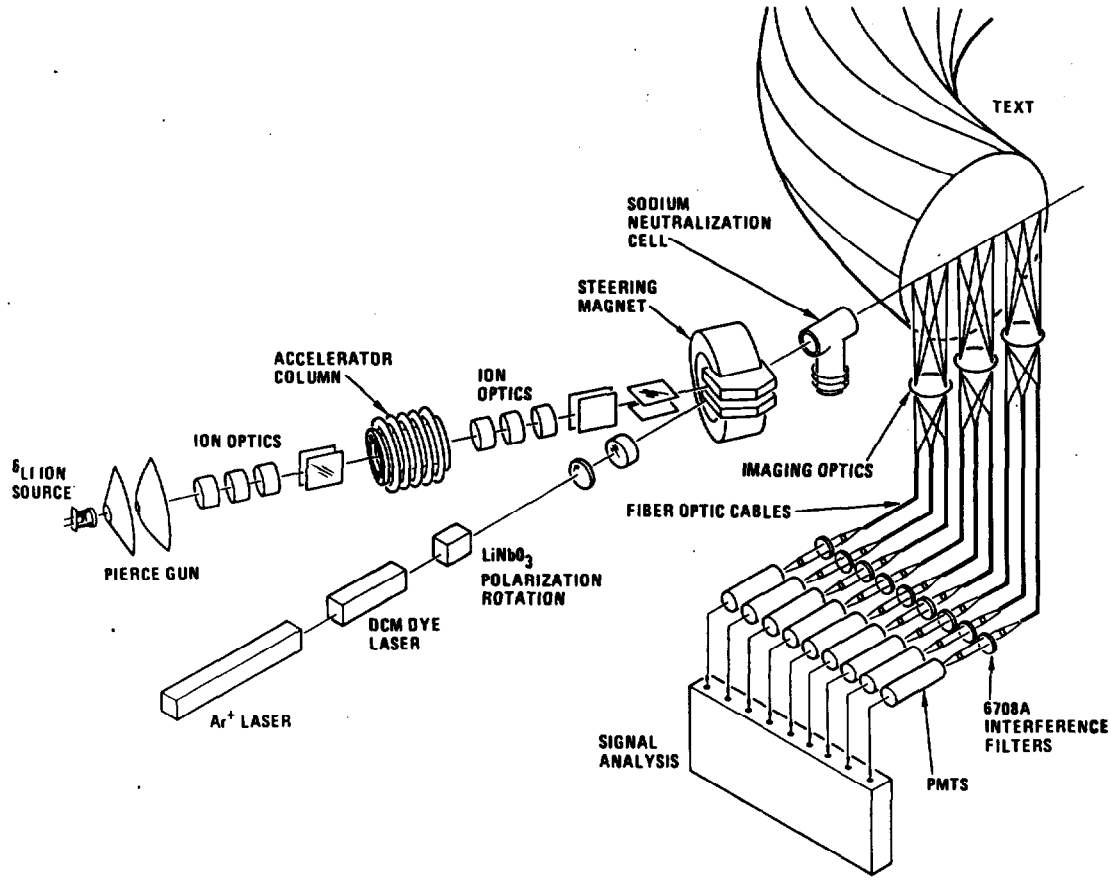

Figure 33: Combination of lithium beam and fluorescence techniques in TEXT (West 1986)

7.6 The motional Stark effect

Energetic neutral hydrogen beams have much better penetration in large, dense plasmas than lithium beams and moreover suitable sources have been extensively developed for plasma heating. The motion of the beam atoms in the tokamak magnetic field, induces an effective electric field $\mathbf{E} = \mathbf{v} \times \mathbf{B}$ in their rest frame. This electric field, typically 4 MVm^{-1} for a beam energy of 50 keV and a magnetic field of 1.5 T, induces a Stark splitting in the Balmer α emission line (λ = 659.1 nm) that is much larger than the Zeeman splitting. The pitch-angle of the magnetic field, and thus the poloidal field component and safety factor $q(r)$ are determined by measuring the direction of polarization of the Stark σ components. This effect was observed in JET using a heating neutral beam (Boileau *et al* 1989) and has been developed into a working diagnostic to measure $q(r)$ in the PBX-M and TFTR tokamaks (Levinton *et al* 1989 and 1990). This technique promises to become a standard diagnostic on many tokamaks during the next few years.

Despite extensive studies over the past decade, the basic plasma processes responsible for the anomalous transport of energy and particles in magnetically confined plasmas remains unknown. One possibility is that small amplitude fluctuations may be involved but these are difficult to detect. Beam-emission spectroscopy is a newly developed technique for measuring density fluctuations in a high temperature tokamak plasma by observing the fluctuations in the intensity of light emitted by an injected neutral hydrogen beam as it interacts with the plasma. This diagnostic has been developed on the PBX-M and TFTR tokamaks using a powerful (5 MW, 100 keV) deuterium heating beam (Paul and Fonck 1990, Fonck, Duperrex and Paul 1990). The deuterium Balmer α line (λ = 656.1 nm) is used and excitation is due primarily by collisions with plasma electrons and ions. The beam is viewed at an angle between 30° and 60°. As in charge-exchange spectroscopy, the measurement is localized to the volume where the spectrometer sight-line intersects the beam. This spatial localization is one of the principle advantages of beam-emission spectroscopy compared to other fluctuation diagnostics. The emission from the beam is Doppler shifted by up to 6 nm enabling the spectrometer to reject unshifted D_α radiation from the plasma edge, nearby impurity emission lines and even light from neighboring beams that are viewed at different angles.

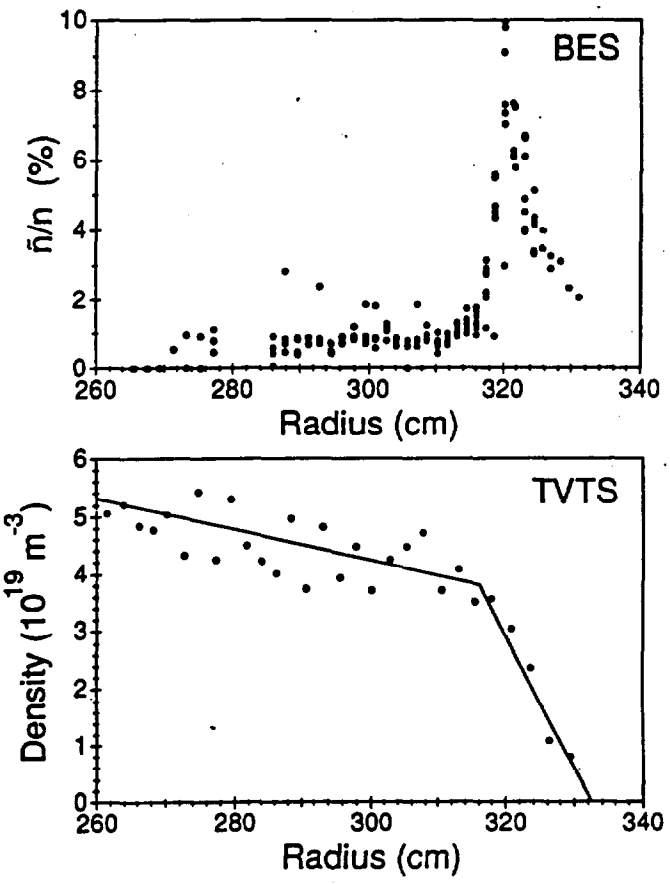

Figure 34: The relative amplitude of density fluctuations in a TFTR L–mode plasma measured with beam–emission spectroscopy showing a large increase in fluctuation amplitude in the region where the density gradient (measured with Thomson scattering) is steepest (Fonck 1992).

Some results from the TFTR tokamak demonstrating the potential of this new diagnostic technique, are shown in figure 34. The density fluctuations have a frequency spectrum that decreases monotonically to about 50 kHz. Their relative amplitude, $\tilde{n}/n$, is plotted as a function of radius in the plasma poloidal cross-section. In the plasma core, the density fluctuations have small amplitude, typically $\tilde{n}/n < 1\%$ but the amplitude increases substantially at the plasma edge to about 10%. The radial correlation length of the density fluctuations is about 50 mm in the core, falling to about 10 mm at the edge. further studies are required to establish the relationship between these fluctuations and the plasma transport processes.

7.8 X–ray diode arrays

X-ray diagnostics have a very important application for diagnosing temperature fluctuations. Silicon diodes are used to detect the flux of x-rays rather than the energy of single photons. Coarse energy resolution can be provided by thin metallic foil filters. Used in this way, the diode detectors can be sensitive with a time resolution of a few μs to temperature fluctuations with amplitudes of a few eV in plasmas with mean temperatures of several KeV. The detectors can be used singly, but are most effective when used in large arrays to view the plasma through a collimating aperture, forming in effect an X-ray imaging system. The most recent applications use compact photo-diode arrays that can be placed close to the plasma (Granetz 1991). A system planned for the new ALCATOR C-MOD tokamak will have five arrays, each containing 38 detectors (figure 35).

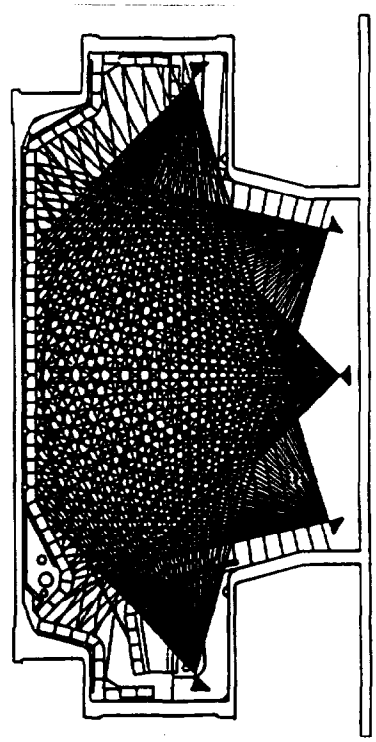

Figure 35: Arrangement of 5 arrays of X–ray detectors being installed in Alcator C–MOD (Granetz 1991)

Each diode detector measures the integral of the X-ray emission along its line-of-sight. Computerized tomographic inversion techniques are used to reconstruct the X-ray emissivity. In most cases the X-ray emissivity is directly related to the electron temperature. These techniques have been developed to a high degree of sophistication and are routinely used to study the spatial structure and temporal development of temperature fluctuations related to internal instabilities in tokamaks. These techniques have found important applications in studies of sawteeth (figure 23) and disruptions. Figure 36 shows profiles of the soft X-ray emission observed in JET shortly before a disruption (Wesson *et al* 1989). The emission is seen to be "eroded" on one side but initially the other side remains unaffected. Electron cyclotron emission measurements show that the drop in X-ray emission is consistent with a fall in electron temperature.

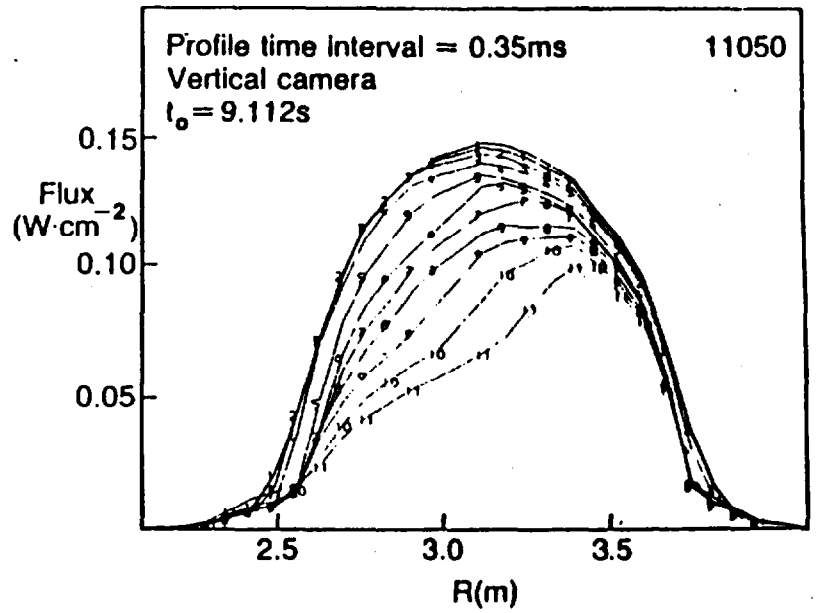

Figure 36: A sequence of x-ray emission profiles showing erosion of the temperature profile before a disruption. The profiles are plotted at intervals of 950 μs (Wesson et al 1989)

A soft X-ray imaging system has been used in JET to study perturbations at the rational q surfaces following the injection of small pellets of solid deuterium (Weller *et al* 1987, Gill *et al* 1992). These pellets, with diameters of a few mm, each containing 2.2×10^{21} to 4.5×10^{21} atoms, are injected radially in the equatorial plane with velocities ≈ 1 kms^{-1} in order to refuel the plasma core. The pellet is ablated as it penetrates the plasma and immediately after the injection an unexpected and very localized density and temperature perturbation is observed. The perturbation has the topology $m = 1$, $n = 1$ and is clearly associated with the $q = 1$ magnetic surface (figure 37). A similar structure with $m = 3$, $n = 2$ associated with the $q = 3/2$ surface is also seen. The temperature and density in the region of the perturbation have been

measured with electron cyclotron emission and with far infra-red interferometry respectively. The density inside the perturbed region can be as large as twice that in the surrounding plasma, although the total number of particles in the perturbation is only $\approx 1\%$ of the particles injected with the pellet. The perturbation lasts for a long time (> 2 s) and can survive drastic changes in the plasma including a sawtooth collapse. The long lifetime of the perturbation allows the position of the $q = 1$ magnetic surface to be followed during a sawtooth cycle.

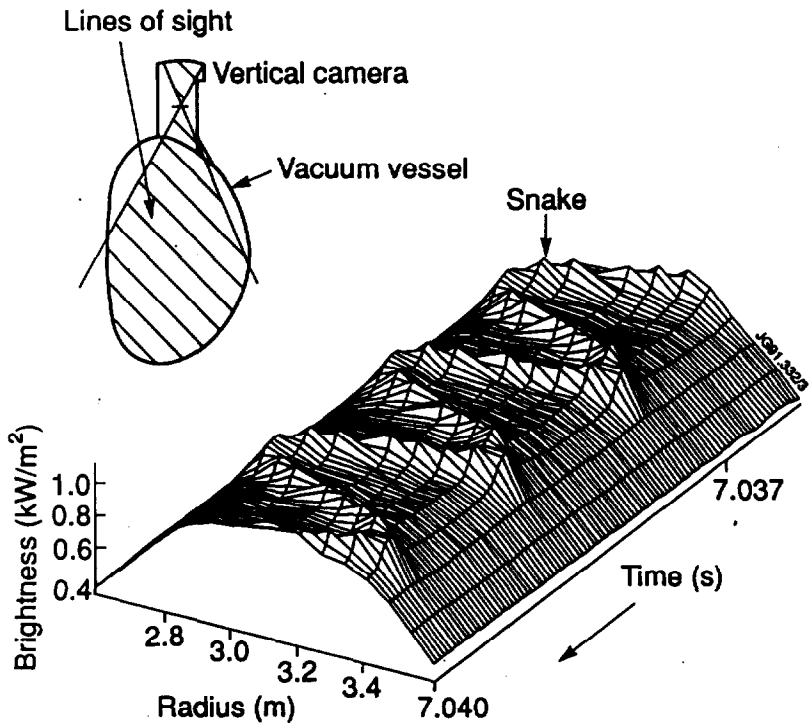

Figure 37: The "snake" perturbation associated with the $q = 1$ rational magnetic surface in JET. The pattern is formed by a small region of enhanced emission rotating through the field of view (Gill et al 1992).

8. Particle beam techniques

Although hot fusion plasmas are almost completely ionized, they contain a small density of neutral atoms in the plasma that can be used for diagnostic purposes. There are three main sources of neutrals in a fusion plasma: gas introduced at the plasma edge for refueling; pellets of solid hydrogen fired into the plasma at high velocity for refueling or diagnostic purposes; energetic neutral beams that are injected in order to heat the plasma or for diagnostics. In a discharge which is refueled by gas introduced at the plasma edge, each cold neutral gas molecule is dissociated by the *Franck–Condon* process into a neutral atom and an ion. The neutral atom is then either *ionized* by electron impact or *charge–exchanged* by collision with a plasma ion. In the charge-exchange process the captive electron is transferred from the atom to the ion with little change to the energies and momenta of the nuclei.

Thus the net effect is that the original "cool" neutral distribution at the plasma edge is replaced by a "hotter" neutral distribution with a temperature characteristic of the plasma ions deeper in the plasma. These hot neutrals, unconfined by the magnetic field, can move freely and penetrate deeper into the plasma via a cascade of charge-exchange collisions with progressively hotter plasma ions. Charge-exchange collisions between neutrals and plasma ions produces energetic neutrals that can escape from the plasma and carry with them information about the energy distribution of the plasma ions (Afrosimov and Kislyakov 1982, Kislyakov 1986).

8.1 Passive neutral particle emission

Neutral particles emitted from a fusion plasma are usually detected by being first reionized by collisions in a neutral gas cell or in a thin foil. The secondary ions are then energy and momentum analyzed in a combination of electric and magnetic fields. Various configurations of field analysers have been tried by different workers. The earliest neutral particle diagnostics used secondary electron or gridded electron multipliers and were usually limited to a single channel, so that the energy spectrum had to be built up either on a shot-to-shot basis or by sweeping the analyzer voltage as a function of time. Substantial improvements have resulted from the application of channel electron multipliers which are robust, compact and very sensitive. Their small physical size allows them to be used in arrays. When used with suitable combinations of compact electric and magnetic field analyzers, this permits the simultaneous measurement of energy spectra of mixed ion species. This is particularly useful in separating the thermal- and fast-ion spectra when a neutral beam of one species (eg. hydrogen) is used to heat a target plasma of a different species (eg. deuterium).

The application of neutral particle diagnostics to experiments nearing reactor conditions, requires particle analyzers that can operate in a high background flux of neutrons and gamma radiation. The operation of a conventional neutral particle analyzer system on JET has been seriously affected by neutron-induced background noise. A new time-of-flight technique where the random background can be discriminated by standard coincidence techniques has been developed (Corti *et al* 1991). Neutrals are ionized in a gas stripping cell and energy-analyzed with a cylindrical electrostatic plate system. The ions then pass through a thin carbon foil (1 $\mu g/cm^2$), producing secondary electrons that are detected by a channeltron which starts a coincidence timer with a set of programmed delays (in the range 10 to 400 ns) corresponding to different masses with the selected energy. The timer is stopped when the ions reach a

second channeltron after a flight path of 120 - 300 mm. The JET system has 15 energy channels covering the range 0.5 to 200 keV for hydrogen, deuterium and helium neutrals.

The flux of neutrals emanates from all points of the plasma along the chord viewed by the detector. Consequently the measured spectrum has to be unfolded to give the radial profile. When the plasma density and diameter are such that the atom mean-free-path is comparable to the plasma diameter, the hottest region of plasma in the line-of-sight contributes most of the highest energy neutrals and thus the high-energy portion of the neutral spectrum is characteristic of the highest temperature. This is the classic method of passive neutral particle analysis which has been used for many years to determine central ion temperatures in small and medium-sized tokamaks. The flux of neutrals from the core of larger or denser plasmas is strongly reduced by two effects: the neutral density in the core is small because neutrals from gas refueling at the edge do not easily penetrate; the few neutrals produced at the plasma core are further attenuated before they reach the edge. Under these conditions the neutral spectrum is dominated by particles from the edge and it is difficult to extract information about the core. It is possible to estimate the core temperature using an analysis code which models the neutral atom transport in the plasma. Measurements of the core plasma are improved when a neutral particle beam is used to enhance the neutral atom density in the core as discussed below.

8.2 Active beam techniques

The naturally occurring flux of charge-exchange neutrals emitted by the plasma can be increased considerably by injecting an energetic beam of neutrals which can penetrate to the core. This also improves the spatial resolution by defining a sample volume at the intersection of the beam and the line-of-sight of the detector. The ion temperature profile can be determined by making a series of measurements along chords that intersect the beam. The resolution can be further improved by modulating the intensity of the injected beam and using phase-sensitive detection techniques. Although there are complications, for example the spatial resolution is reduced because the probing beam is surrounded by a "halo" of secondary charge-exchanged neutrals, the active beam diagnostic is much improved for large plasmas compared to the passive charge-exchange method. A probing beam which is sufficiently energetic (typically > 40 keV) and intense (typically several Amperes) to penetrate and illuminate a large plasma is a substantial undertaking but there has been considerable development of beam technology for plasma heating purposes.

8.2.1 Fast ion distributions. Several diagnostic methods based on beams are being developed to study the energy distribution of alpha particles in fusion plasmas. Single charge-exchange leads to an excited He^+ ion which can be diagnosed spectroscopically. Double charge-exchange leads to fast neutral helium atoms which can be detected and energy-analyzed after they escape from the plasma. However the cross-sections for these charge-exchange reactions are significant only if the velocity of the probing beam is close to that of the alpha particle. Consequently very high energy probing beams (2.6 MeV ^3He or 5.5 MeV Li) would be required to diagnose the full energy distribution of alpha particles in a fusion plasma. Lower energy beams in the range 40 to 200 keV where higher beam intensity would partly compensate for the reduced cross-section could be used to access the lower energy range of the alpha particle distribution.

8.3. Rutherford scattering

Ion temperatures have been measured from the broadened energy spectrum of a beam of energetic helium ions that has been elastically scattered from the plasma. This method was first applied on the T4 tokamak several years ago and more recently has been used on the JT-60 and TEXTOR tokamaks (van Blokland 1991).

8.4 Heavy–ion beams

Heavy-ion beam diagnostics have been used in several fusion experiments to measure the plasma density, the electrostatic potential, the poloidal magnetic field and the fluctuations of these quantities. The heavy-ion beam is the only diagnostic method capable of measuring plasma potential in the plasma interior, although Langmuir probes can be used at the plasma edge. The correlation between the density and potential fluctuations is required in order to calculate the flux of particles transported by electrostatic fluctuations.

A beam of singly-charged thallium or caesium ions is accelerated to a high energy, typically 100 to 500 keV, so that the Larmor radius of the heavy ions in the toroidal field of the tokamak is larger than the minor radius of the plasma. The primary beam is ionized along its path by collisions with plasma electrons:

$$Tl^+ + e^- \Rightarrow Tl^{++} + 2e^-.$$

The ionization introduces negligible momentum or energy transfer to the beam

ions because of the large mass difference between the heavy ions and an electron, but the energy of the secondary ions, when they leave the plasma, is changed relative to the energy of the primary ions by an amount $e\phi$, where ϕ is the electrostatic potential of the plasma at the point of ionization. The Larmor radius of the secondary ions is half that of the primary ions so that the beams diverge. The location of the sample volume in the plasma is determined by the intersection of the trajectories of the two beams. This can be calculated knowing the energy of the primary beam, the magnitude of the confining magnetic fields and the beam geometry. The secondary ions are detected with an energy analyzer which determines their energy, flux and displacement in the toroidal direction. The plasma potential, density and poloidal magnetic field are determined from these three measured quantities.

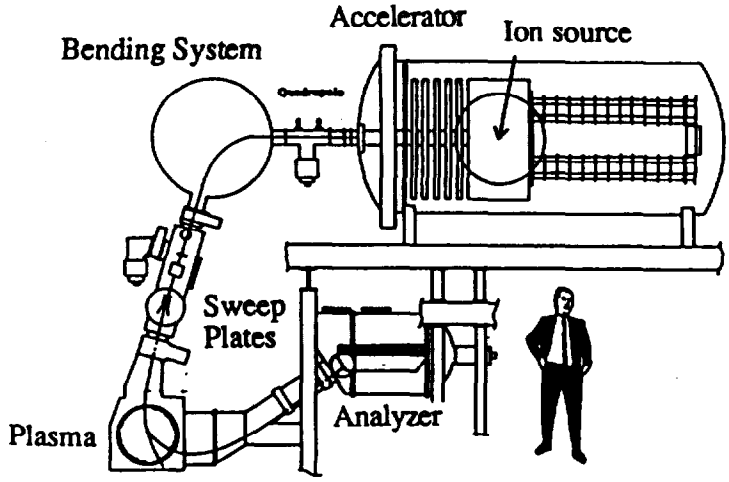

Figure 38: Schematic of the TEXT tokamak installed on the heavy–ion beam diagnostic (Wootton and Schoch 1991).

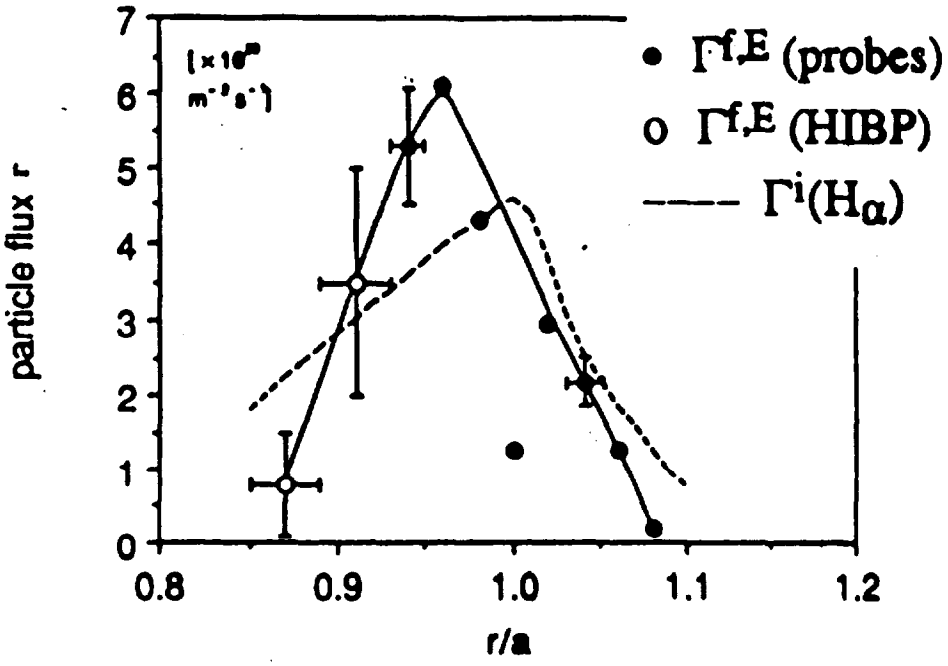

Figure 39: Comparison of the particle fluxes determined by the heavy ion beam and Langmuir probe diagnostics at the edge of TEXT and fluxes measured spectroscopically (Wootton and Schoch 1991).

The large physical size of the heavy-ion beam diagnostic is apparent from figure #38. This diagnostic has not been applied to any of the large tokamaks because beam energies of several MeV would be required for adequate beam penetration. Figure #39 shows some of the results obtained in the TEXT tokamak. The particle fluxes calculated from the density and potential fluctuations measured with the heavy-ion beam diagnostic and similar quantities calculated from Langmuir probe measurements are compared with the particle flux determined by spectroscopic measurements. These results indicate that electrostatic fluctuations make a major contribution to particle transport at the plasma edge.

9. Fusion Products

Fusion products are being used increasingly for diagnostic purposes as plasma conditions approach the fusion goal. The principal fusion products are: neutrons (2.45 MeV energy from dd reactions and 14 MeV from dt reactions); ^{3}He ions (0.82 MeV from dd reactions); ^{4}He ions (3.65 MeV from dt reactions); and protons (14.6 MeV from d^{3}He reactions). Reaction rates cover a wide range, from 10^{10} s^{-1} to 10^{17} s^{-1} in hydrogen and deuterium plasmas and will extend (in JET and TFTR) up to 10^{19} s^{-1} in tritium plasmas.

9.1 Neutron detectors

Because neutrons are uncharged, detection techniques must be based either on nuclear transformation reactions or on neutron scattering. The full range of available techniques includes: track recorders (requiring optical examination after irradiation); dosimeters (giving time-integrated responses); counters (with no energy discrimination); simple spectrometers; and spectrometers housed in collimators (usually based on neutron elastic scattering methods). Whilst many of these techniques have been extensively developed for nuclear physics applications, there are several factors relevant to the fusion application which require special consideration. These include the need for detectors: to be insensitive to magnetic fields; to have low response to gamma radiation; to be tolerant of high radiation doses; to be insensitive to electromagnetic interference; to be tolerant to mechanical vibrations; and to be capable of operating at high repetition rates (Jarvis 1991).

The time dependence of the neutron yield is measured with detectors that utilize the reactions of certain nuclides (^{3}He, ^{6}Li, ^{10}B, and ^{235}U) with thermal neutrons. The incident neutrons are thermalized in a suitable moderator, (for example polyethylene), and consequently the detector becomes

insensitive to their energy. A wide range of neutron yields is covered using several detectors with different sensitivities. The spatial profile of the neutron yield is measured using arrays of time-resolving detectors inside multi-aperture collimators. When the neutron yield is sufficiently high, the time resolution can be fast enough to follow transient events such as a sawtooth collapse (figure #40). An alternative technique for measuring neutron yields is foil activation. Foils are exposed to the neutrons and then removed to a remote counting station where the decay transitions can be recorded in an environment free from mechanical, electrical, magnetic and radiation interferences. The foil technique is used to calibrate other detectors. It can also be used to determine energy spectra with coarse energy resolution by exposing a package of several foils with a suitable range of activation energies. The energy resolution is insufficient for temperature measurements but is adequate to eliminate neutrons from non-fusion sources.

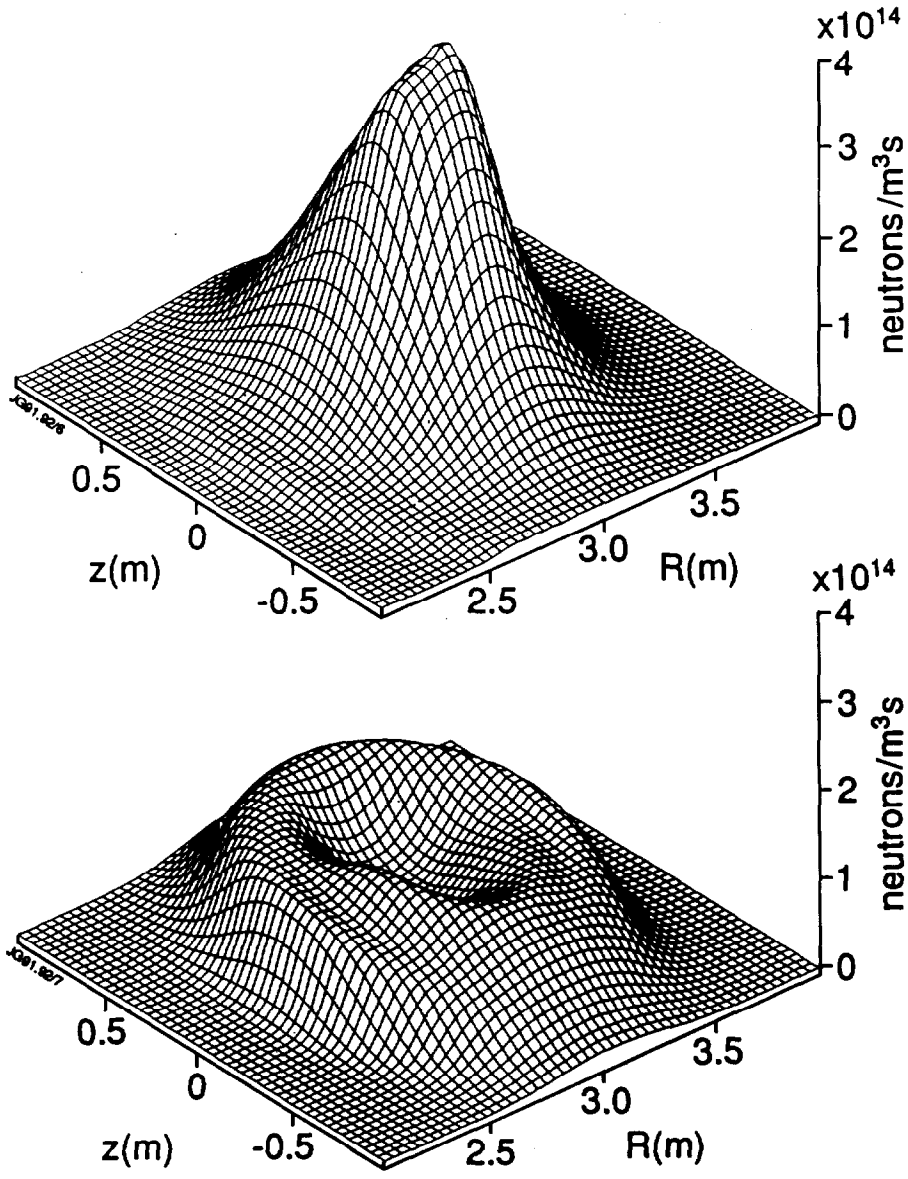

Figure 40: Tomographic reconstructions of neutron emission profiles before and after a sawtooth collapse in JET.

Ion temperatures can be determined from the neutron yield. In a Maxwellian deuterium plasma, the fusion reaction rate $R_{dd} \approx n_d^2 T_i^x$ (where x depends on the ion temperature T_i and is approximately 4 for $T_i = 3$ keV). Because of this strong dependence on temperature, the total neutron yield is determined mainly by the ion temperature in the plasma core and is relatively insensitive to the deuteron density and to the profile shapes. However since most of the neutrons are produced by ions on the tail of the Maxwellian distribution, the neutron yield and the derived ion temperature, are extremely sensitive to any non-thermal ions. For example, when a deuterium plasma is heated by a deuterium neutral beam, the neutron yield from the fast, injected ions will be much larger than that from the thermal ions. Neutron spectrometry is a more reliable way of determining the ion energy distribution and temperature. The intrinsic energy peak of the neutrons from the fusion reaction is broadened slightly by the additional kinetic energy of the colliding deuterons and by the transformation from the centre- of-mass frame of reference. Both the broadening and the yield depend on the temperature, so that both the resolution and the sensitivity of a spectrometer must be matched to the appropriate temperature range. It is particularly difficult to measure ion temperatures lower than about 5keV because spectrometers with sufficiently high resolution would be too insensitive for the low yields. Consequently the techniques and applications of neutron spectrometry have only started to be developed in a major way in the last few years with the advent of large, hot fusion experiments such as JET and TFTR.

One technique for high resolution spectrometry utilizes transformation reactions of the type $n + {}^3He \Rightarrow p + t$ where all of the free energy is carried by charged particles and therefore can be measured. Ion temperatures have been measured in deuterium plasmas in JET using ^{3}He ionization chambers. Although similar detectors have been used previously in the Alcator and PLT tokamaks, neutron fluxes were too low in the smaller tokamaks to give good data. The JET detector is a cylindrical, gridded chamber filled with a mixture of helium, argon and methane at a pressure of 10 bar. The plasma is viewed vertically from a distance of about 20 m through a 0.2 m diameter hole in a 2 m thick concrete roof. This type of detector is very sensitive to thermal and epithermal neutrons so that only about 3% of the recorded events are due to 2.4 MeV neutrons. The maximum count rate of a ^{3}He chamber is a few kHz because relatively long time constants are required in order to optimize the energy resolution. Consequently it takes several seconds to measure a spectrum with sufficient accuracy.

Other types of high-resolution spectrometer are based on the elastic scattering of neutrons by protons. The direction of motion of the incident neutron is defined with a suitable collimator and the energy and direction of either the scattered neutron or the recoiling proton (or both of these) are measured. The instrument has to be surrounded by a thick screen to reduce the background radiation of gamma rays and neutrons. The shield and collimator are usually made of a combination of polyethylene, concrete and steel. The shield for a typical 14 MeV spectrometer could weigh up to 100 tonnes. There are several alternative arrangements to measure the recoiling proton. The simplest system is the "in-line" geometry where the collimated neutron beam strikes a thin polyethylene target and the protons are detected in the forward direction. The energy resolution depends on the energy resolution of the proton detector, the thickness of the scattering foil and the geometry. A disadvantage of this system is that the detector is in the beam of unscattered neutrons. An alternative approach is to determine the energy of the scattered neutron by measuring its time-of-flight. This method was first applied to pulsed neutron sources where the source itself provides the start signal and there is a single detector at a suitable distance. When the source of neutrons is a quasi-continuous plasma, it is necessary to use two detectors. The first detector is a hydrogenous scintillator which records all the recoil protons, and the second detector determines the time-of-flight. A diagnostic based on this principle has been operated on JET. The features of both proton recoil and time-of-flight methods are combined in the so called "associated particle" spectrometer. This employs a proton recoil counter at a small angle, typically 20^0, so as to be out of the collimated flux of neutrons. The energy resolution is improved by also measuring the neutron energy via the time-of-flight method. Such a system is being constructed for use at JET to diagnose 14 MeV neutrons from d - t plasmas.

9.3. Charged fusion products

Charged fusion products (tritons, protons and alpha-particles) are confined on particle orbits within the plasma and can be detected directly only when they escape. This is usually after their energy has been degraded. In one application, 3 MeV protons from d(d,p)t reactions have been used to measure local gradients of ion temperature in PLT (Lovberg and Strachan 1990). Local fusion reaction rates were determined from the fluxes of protons originating from different radial points in the plasma. These were measured with a single surface barrier detector using an array of collimators, each of which was covered with a thin aluminium foil of a different thickness, so that different proton orbits could be identified by the residual proton energies. Ion

temperature gradients were derived from the differences in the fusion reaction rates and were used in energy balance calculations to determine the ion thermal diffusivity.

10. Edge & Surface Diagnostics

The outer, annular region between the last closed magnetic surface and the wall is usually called the *scrape–off layer*. Energy and particles from the hot central plasma core are transported to the edge by a variety of processes and ultimately diffuse through the scrape-off layer onto material surfaces at the limiter or divertor. Some particles are *recycled* and return to the plasma to be re-ionized and re-heated. Plasma bombardment of these material surfaces releases impurities which also become ionized and heated as they penetrate the core plasma. The boundary plasma has a strong influence on the purity and confinement properties of the entire plasma, though in general it is poorly diagnosed. In many ways it is more difficult to diagnose the edge than the core plasma (McCracken 1982, 1986, Stott 1991). Spatial scale lengths are much shorter in the boundary than in the core and better resolution is needed. A further complication is introduced by toroidal and poloidal asymmetries, which can be quite significant in the scrape-off layer, whereas the core plasma parameters usually have the same value everywhere on the same magnetic surface. Many of the diagnostic techniques that have been developed for the core plasma cannot be used or are less effective in the less dense and cooler boundary plasma. In recent years some techniques have been extended (examples include high-resolution Thomson scattering, electron cyclotron emission and microwave reflectometer systems to measure boundary densities and temperatures) and some new techniques, like fluorescence spectroscopy to measure neutral impurity densities, have been developed.

10.1 Langmuir probes

Probes are widely used at the outer edge where densities and temperatures are too low for other methods and where the power flux is low enough for the probes to survive. Langmuir probes are used to measure electron densities and temperatures. The simplest form of probe consists of a single electrode inserted into the plasma and biased at a variable potential. When the probe is negative with respect to the plasma it collects ions, when positive it collects electrons. The electron temperature can be determined from the slope of the current versus bias-voltage characteristic. These probes can be mounted on movable drives or incorporated into the actual limiter or divertor surfaces. Other more sophisticated types of electrical probe have been

developed (Manos and McCracken 1986). Examples include heat flux probes which measure the power flux using a thermocouple as one of the electrodes in a Langmuir probe, gridded electrostatic analyzers and miniaturized mass spectrometers to measure impurity distributions (Mathews 1989).

10.2 Surface analytical techniques

The erosion and deposition of hydrogen and impurities in the scrape-off layer are measured with surface collector probes which are exposed to the plasma for a fixed time and then withdrawn it to a remote chamber for analysis. Good time resolution (typically 10ms) can be achieved by using rotating cylindrical collectors behind a fixed aperture slit so that the radial position around the cylinder corresponds to time and axial position corresponds to radial position in the scrape-off layer. The subsequent surface analysis techniques (Zuhr, Roberto and Appleton 1984) are well-developed in other branches of physics. They include Auger electron spectroscopy (AES), secondary-ion mass spectroscopy (SICS), Rutherford back-scattering (RBS), proton-induced X ray emission (PIXE) and nuclear reaction analysis (NRA). These techniques are very sensitive and have the advantage that the sample can be examined away from the high electrical noise and radiation environment of the fusion experiment. With a mixture of these techniques all impurity masses can be investigated. Low-Z collectors such as carbon or silicon are used to investigate metallic impurities and in this case it is possible to transfer the samples from the fusion device to the analysis system via the atmosphere. However a vacuum transfer is necessary to avoid contamination of samples which will be used to study low-Z impurities such as carbon or oxygen. Several tokamak experiments have surface diagnostic systems which are directly connected so that the collector probe can be transported to the analysis system without the risk of contamination by exposure to air.

10.3 Infra–red imaging

The power flux to the limiters and other surfaces surrounding the plasma can be estimated with thermocouples but usually the time resolution is poor due to thermal inertia. The surface temperature can be measured by infra-red imaging cameras. These methods have been developed also as surveillance devices to detect localized heating or hot spots which could cause damage.

11. Summary and future prospects

Progress in fusion research has always been limited by the difficulty of measuring the many plasma quantities that are needed to characterize the plasma and to attempt to understand its behavior. Most advances in diagnostic techniques have had a significant impact on progress in fusion research. In this review I have tried to cover the main developments that have taken place during recent years. This is a wide field to cover even when restricted to tokamaks which have emerged as the dominant configuration in magnetic confinement. Of necessity, this review has been selective in quoting examples of particular techniques from among the many excellent groups working on diagnostic development and application. It has also been selective in quoting examples of the impact of specific diagnostic methods. There has been continual progress in the refinement and improvement of the well-established techniques, as well as the introduction of new methods. These advances have been stimulated by various factors including improved data handling methods and by the requirements of the present generation of large tokamak experiments which have stimulated the development of diagnostic systems with improved reliability, greater accuracy and many more measurement channels. There is no doubt that the next generation of fusion experiments will stimulate many comparable advances in diagnostics, in particular measurements of alpha particles and other fusion products will be needed and it will be necessary to develop new techniques to replace those which are not compatible with the environment of a fusion reactor.

References

Afrosimov V V and Kislyakov A I 1982 *Diagnostics for Fusion Reactor Conditions*, ed P E Stott, D K Akulina, G G Leotta, E Sindoni and C Wharton (Oxford: Pergamon) vol I pp 289-310

Baker D R and Lee S T 1978 *Rev. Sci. Instrum.* **49** 919-22

Behn R *et al* 1989 *Phys. Rev. Lett.* **24** 2833-6

Boileau A, von Hellerman M, Mandl W *et al* 1989 *J. Phys B: At. Mol. Opt. Phys.* **22** L145-

Braams B J 1991 *Plasma Phys. Contr. Fusion* **33** 715-48

Bretz N *et al* 1978 *Appl. Opt.* **17** 192-202

Brower D L *et al* 1990 *Phys. Rev. Lett.* **65** 337-40

Bruneau J L and Gil C 1991 Private communication

Callen J D and Jahns G L 1977 *Phys. Rev. Lett.* **38** 491-4

Campbell D J, Edwards A W and Pearson D 1989 *Controlled Fusion and Plasma Physics (Proc 16th European Conf. Venice)* Europhysics Conf. Abstracts vol 13B part II pp 509-12

Carstrom T N *et al* 1991 *14th IEEE Symposium on Fusion Engeneering, San Diego* (to be published)

Corti S, Bracco G, Moleti A *et al* 1991 *Diagnostics for Contemporary Fusion Experiments*, ed P E Stott *et al* pp 477-96

Costley A E 1982 *Diagnostics for Fusion Reactor Conditions*, ed P E Stott, D K Akulina, G G Leotta, E Sindoni and C Wharton (Oxford: Pergamon) vol I pp 129-65

Costley A E 1986 *Basic and Advanced Diagnostic Techniques for Fusion Plasmas*, ed P E Stott, D K Akulina, G G Leotta, E Sindoni and C Wharton (Brussels: CEC) vol II pp 379-96

Costley A E, Cripwell P, Prentice R and Sips A C C 1990 *Rev. Sci. Instrum.* **61** 2823-8

Costley A E 1991 *Diagnostics for Contemporary Fusion Experiments*, ed P E Stott *et al* pp 113-134

de Haas J C M, O'Rourke J, Sips A C C and Lopez Cardoza N J 1991 *Nucl. Fusion* **31** 1261-74

de Michelis C 1986 *Basic and Advanced Diagnostic Techniques for Fusion Plasmas*, ed P E Stott, D K Akulina, G G Leotta, E Sindoni and C Wharton (Brussels: CEC) vol I pp 83-118

Equipe TFT 1978 *Nucl. Fusion* **18** 647-731

Fishpool G 1992 *Private communication*

Fonck R J, Duperrex P A and Paul S F 1990 *Rev. Sci. Instrum.* **61** 3487-95

Fonck R J 1992 Private communication

Forrest M J, Carolan P G and Peacock N J 1978 *Nature* **271** 718-22

Gentle K W 1988 *Physics Fluids* **31** 1105-10

Gill R D, Edwards A W, Pasini D and Weller A 1992 *Nuclear Fusion* (submitted)
Gottardi N 1979 *J. Appl. Phys.* **50** 2647-51

Gowers C 1991 *Diagnostics for Contemporary Fusion Experiments*, ed P E Stott *et al* pp 261-82

Granetz R S 1991 *Diagnostics for Contemporary Fusion Experiments*, ed P E Stott *et al* pp 407-24 and 425-38

Gusev V K 1986 *Basic and Advanced Diagnostic Techniques for Fusion Plasmas*, ed P E Stott, D K Akulina, G G Leotta, E Sindoni and C Wharton (Brussels: CEC) vol II pp 497-516

Hawryluk R *et al* 1987 *Plasma Physics and Controlled Nuclear Fusion Research (Proc 11th Int. Conf. Kyoto)*, (Vienna: IAEA) vol 1 51-64

Heijnen S H, Hugenholtz C A J, Pavlo P, van der Pol M J and Žáček F 1991 *Diagnostics for Contemporary Fusion Experiments*, ed P E Stott *et al* pp 747-54

Hill K W *et al* 1986 *Basic and Advanced Diagnostic Techniques for Fusion Plasmas,* ed P E Stott, D K Akulina, G G Leotta, E Sindoni and C Wharton (Brussels: CEC) vol I pp 201-27

Howard J 1989 *Proc 4th Int. Symposium on Laser Aided Plasma Diagnostics,* (Fukuoaka, Japan) 310-315

Hutchinson I H 1987 *Principles of Plasma Diagnostics* (Cambridge: Cambridge University Press)

Ida K *et al* 1991 *Phys. Fluids* **B3** 515-

Isler R C 1987 *Physica Scripta* **35** 650-61

Isler R C 1991 *Diagnostics for Contemporary Fusion Experiments*, ed P E Stott *et al* pp 357-74

Isler R C 1992 Private communication

Jarvis O N J 1991 *Diagnostics for Contemporary Fusion Experiments*, ed P E Stott *et al* pp 541-54 and 555-72

Johnson D *et al* 1985 *Rev. Sci. Instrum.* **56** 1015-17

Kadota K *et al* 1982 *Jpn. J. Appl. Phys.* **21** L260-2

Kim S K, Brower D L , Peebles W A and Luhmann N C, 1988a *Rev. Sci. Instrum.* **59** 1550-5

Kim S K *et al* 1988b *Controlled Fusion and Plasma Heating (Proc. 15th European Conf. Dubrovnik)* Europhysics Conf. Abstracts vol 12B part I 187-90

Kislyakov 1986 *Basic and Advanced Diagnostic Techniques for Fusion Plasmas,* ed P E Stott, D K Akulina, G G Leotta, E Sindoni and C Wharton (Brussels: CEC) vol II pp 623-34

Lasalle J and Platz P 1979 *Appl. Opt.* **18** 4124-33

Levinton F M, Fonck R J, Gammel G M *et al* 1989 *Phys. Rev. Lett.* **63** 2060-63

Lopez Cardoza N J *et al* 1988 *Plasma Physics Cont. Fusion* **32** 983-98

Lovberg J and Strachan J D 1990 *Nuclear Fusion* **30** 2533-44

McCracken G M 1982 *Diagnostics for Fusion Reactor Conditions*, ed P E Stott, D K Akulina, G G Leotta, E Sindoni and C Wharton (Oxford: Pergamon) vol I pp 419-72

McCracken G M 1986 *Basic and Advanced Diagnostic Techniques for Fusion Plasmas,* ed P E Stott, D K Akulina, G G Leotta, E Sindoni and C Wharton (Brussels: CEC) vol III pp 783-824

McCormick K 1986 *Basic and Advanced Diagnostic Techniques for Fusion Plasmas,* ed P E Stott, D K Akulina, G G Leotta, E Sindoni and C Wharton (Brussels: CEC) vol II pp 635-58

McCormick K, Kick M and Olivain J 1977 *Proc 8th European Conf. on Controlled Fusion and Plasma Physics, Prague* **1** p 140

McCormick K, Söldner F X, Eckhartt D *et al* 1987 *Phys. Rev. Lett.* **58** 491-4

Manos D and McCracken G M 1986 *Physics of Plasma–Wall Interactions in Controlled Fusion* eds Post D E and Behrisch R (New York: Plenum)

Manso M E *et al* 1991 *Controlled Fusion and Plasma Physics (Proc 18th European Conf Berlin)* Europhysics Conf. Abstracts vol 15C part I pp 393-6

Mathews G F 1989 *J. Nucl. Mat.* **162-164** 38-50

Mazzucato E 1975 *Report MATT–1151* (Princeton NJ: PPPL)

Mukhovatov V *et al* 1990 *Iter Documenation Series* no 33 (Vienna: IAEA)

Muraoka K and Maeda M 1991 *Diagnostics for Contemporary Fusion Experiments*, ed P E Stott *et al* pp 305-30

Nielsen P 1982 *Diagnostics for Fusion Reactor Conditions*, ed P E Stott, D K Akulina, G G Leotta, E Sindoni and C Wharton (Oxford: Pergamon) vol I pp 225-59

Ochando M A 1991 *Diagnostics for Contemporary Fusion Experiments*, ed P E Stott *et al* pp 439-54

Orlinskiy D V and Magyar G 1988 *Nucl. Fusion* **28** 611-97

Paul S F and Fonck R J 1990 *Rev. Sci. Instrum.* **61** 3496-500

Peacock N, Robinson D C, Forrest M J, Wilcock P D and Sannikov V V 1969 *Nature* **224** 488-90

Peebles W A *et al* 1990 *Rev. Sci. Instrum.* **61** 3509-19

Prentice R, Costley A E, Fessey J A. and Hubbard A E 1986 *Basic and Advanced Diagnostic Techniques for Fusion Plasmas,* ed P E Stott, D K Akulina, G G Leotta, E Sindoni and C Wharton (Brussels: CEC) vol II pp 451-60

Saltzmann H 1986 *Basic and Advanced Diagnostic Techniques for Fusion Plasmas,* ed P E Stott, D K Akulina, G G Leotta, E Sindoni and C Wharton (Brussels: CEC) vol II pp 477-96

Saltzmann H *et al* 1988 *Rev. Sci. Instrum.* **59** 1451-6

Schivell J 1987 *Rev. Sci. Insrum.* **58** 12-

Schubert R *et al* 1990 *Controlled Fusion and Plasma Heating (Proc 17th European Conf Amsterdam)* Europhysics Conf. Abstracts vol 14B part IV pp 1552-55

Sheffield J 1975 *Plasma Scattering of Electromagnetic Radiation* (New York: Academic)

Siegrist M *et al* 1991 *Diagnostics for Contemporary Fusion Experiments*, ed P E Stott *et al* pp 283-304

Simonet F 1985 *Rev. Sci. Instrum.* **56** 664-9

Sindoni E and Wharton C 1978 (eds) *Diagnostics for Fusion Experiments; Proceedings of the Intenational School of Plasma Physics, Varenna* (Oxford: Pergamon)

Sips A C C *et al* 1991 *Nuclear Fusion* **31** 1545-9

Slusher R E and Surko C M 1980 *Phys. Fluids* **23** 472-90

Snipes J A *et al* 1988 *Nucl. Fusion* **28** 1085-97

Soltwisch H 1986a *Basic and Advanced Diagnostic Techniques for Fusion Plasmas,* ed P E Stott, D K Akulina, G G Leotta, E Sindoni and C Wharton (Brussels: CEC) vol II pp 343-60 and pp 361-78

Soltwisch H *et al* 1987 *Plasma Physics and Controlled Nuclear Fusion Research (Proc 11th Int. Conf. Kyoto 1986),* (Vienna: IAEA) vol 1 263-74

Soltwisch H 1989 *Proc 4th Int. Symposium on Laser Aided Plasma Diagnostics,* (Fukuoaka, Japan) 278-83

Soltwisch H 1991 *Diagnostics for Contemporary Fusion Experiments*, P E Stott *et al* pp 75-94

Stott P E 1982a *Diagnostics for Fusion Reactor Conditions*, ed P E Stott, D K Akulina, G G Leotta, E Sindoni and C Wharton (Oxford: Pergamon) vol II pp 403-18

Stott P E 1982b *Diagnostics for Fusion Reactor Conditions*, ed P E Stott, D K Akulina, G G Leotta, E Sindoni and C Wharton (Oxford: Pergamon) vol I pp 187-98

Stott P E, Akulina D K, Leotta G G, Sindoni E and Wharton C 1982 (eds) *Diagnostics for Fusion Reactor Conditions; Proceedings of the International School of Plasma Physics, Varenna* (Oxford: Pergamon)

— 1986 *Basic and Advanced Diagnostic Techniques for Fusion Plasmas; Proceedings of the International School of Plasma Physics, Varenna* (Brussels: CEC)

Stott P E *et al* 1991 *Diagnostics for Contemporary Fusion Experiments ...*

Terry J L, Marmar E S, Howell R B *et al* 1990 *Rev. Sci Instrum.* **61** 2908-13

The JET Team 1991 to be published in *Nuclear Fusion*

Tubbing B J D, Lopez Cardoza N J and van der Weil M J 1987 *Nucl. Fusion* **27** 1843-55

van Blokland A E E *et al* 1992 *Rev. Sci. Instrum.* (submitted)

Veron D 1982 *Diagnostics for Fusion Reactor Conditions*, ed P E Stott, D K Akulina, G G Leotta, E Sindoni and C Wharton (Oxford: Pergamon) vol I pp 199-224

Weisen H *et al* 1989 *Nuclear Fusion* **29** 2187-97

Weller A *et al* 1987 *Phys. Rev. Lett.* **59** 2303-

Wesson J 1987 *Tokamaks* (Oxford: Clarendon)

Wesson J A *et al* 1989 *Nuclear Fusion* **29** 641-66

West W P 1986 *Rev. Sci. Instrum.* **57** 2006-10

Wootton A J 1979 *Nucl. Fusion* **19** 987-90

Wootton A J 1991 *Diagnostics for Contemporary Fusion Experiments*, P E Stott *et al* pp 17-36

Wootton A J and Schoch P M 1991 *Diagnostics for Contemporary Fusion Experiments*, P E Stott *et al* pp 521-40

Woskoboinikow P *et al* 1983 *Proceedings of the Eleventh European Conference on Fusion and Plasma Physics, Aachen* (Petit Lancy: European Physical Society)

Zuhr R A, Roberto J B and Appleton B R 1984 *Nucl. Sci. Appl.* **1** 617-

ANNEX

P.-H. REBUT, A. GIBSON, M. HUGUET, J.M. ADAMS[1], B. ALPER, H. ALTMANN, A. ANDERSEN[2], P. ANDREW[3], M. ANGELONE[4], S. ALI-ARSHAD, P. BAIGGER, W. BAILEY, B. BALET, P. BARABASCHI, P. BARKER, R. BARNSLEY[5], M. BARONIAN, D.V. BARTLETT, L. BAYLOR[6], A.C. BELL, G. BENALI, P. BERTOLDI, E. BERTOLINI, V. BHATNAGAR, A.J. BICKLEY, D. BINDER, H. BINDSLEV[2], T. BONICELLI, S.J. BOOTH, G. BOSIA, M. BOTMAN, D. BOUCHER, P. BOUCQUEY, P. BREGER, H. BRELEN, H. BRINKSCHULTE, D. BROOKS, A. BROWN, T. BROWN, M. BRUSATI, S. BRYAN, J. BRZOZOWSKI[7], R. BUCHSE[22], T. BUDD, M. BURES, T. BUSINARO, P. BUTCHER, H. BUTTGEREIT, C. CALDWELL-NICHOLS, D.J. CAMPBELL, P. CARD, G. CELENTANO, C.D. CHALLIS, A.V. CHANKIN[8], A. CHERUBINI, D. CHIRON, J. CHRISTIANSEN, P. CHUILON, R. CLAESEN, S. CLEMENT, E. CLIPSHAM, J.P. COAD, I.H. COFFEY[9], A. COLTON, M. COMISKEY[10], S. CONROY, M. COOKE, D. COOPER, S. COOPER, J.G. CORDEY, W. CORE, G. CORRIGAN, S. CORTI, A.E. COSTLEY, G. COTTRELL, M. COX[11], P. CRIPWELL[12], O. Da COSTA, J. DAVIES, N. DAVIES, H. de BLANK, H. de ESCH, L. de KOCK, E. DEKSNIS, F. DELVART, G.B. DENNE-HINNOV, G. DESCHAMPS, W.J. DICKSON[13], K.J. DIETZ, S.L. DMITRENKO, M. DMITRIEVA[14], J. DOBBING, A. DOGLIO, N. DOLGETTA, S.E. DORLING. P.G. DOYLE, D.F. DÜCHS, H. DUQUENOY, A. EDWARDS, J. EHRENBERG, A. EKEDAHL, T. ELEVANT[7], S.K. ERENTS[11], L.G. ERIKSSON, H. FAJEMIROKUN[12], H. FALTER, J. FREILING[15], F. FREVILLE, C. FROGER, P. FROISSARD, K. FULLARD, M. GADEBERG, A. GALETSAS, T. GALLAGHER, D. GAMBIER, M. GARRIBBA, P. GAZE, R. GIANNELLA, R.D. GILL, A GIRARD, A. GONDHALEKAR, D. GOODALL[11], C. GORMEZANO, N.A. GOTTARDI, C. GOWERS, B.J. GREEN, B. GRIEVSON, R. HAANGE, A. HAIGH, C.J. HANCOCK, P.J. HARBOUR, T. HARTRAMPF, N.C. HAWKES[11], P. HAYNES[11], J.L. HEMMERICH, T. HENDER[11], J. HOEKZEMA, D. HOLLAND, M. HONE, L. HORTON, J. HOW, M. HUART, I. HUGHES, T.P. HUGHES[10], M. HUGON, Y. HUO[16], K. IDA[17], B. INGRAM, M. IRVING, J. JACQUINOT, H. JAECKEL, J.F. JAEGER, G. JANESCHITZ, Z. JANKOVICZ[18], O.N. JARVIS, F. JENSEN, E.M. JONES, H.D. JONES, L.P.D.F. JONES, S. JONES[19], T.T.C. JONES, J.-F. JUNGER, F. JUNIQUE, A. KAYE, B.E. KEEN, M. KEILHACKER, G.J. KELLY, W. KERNER, A. KHUDOLEEV[21], R. KONIG, A. KONSTANTELLOS, M. KOVANEN[20], G. KRAMER[15], P. KUPSCHUS, R. LÄSSER, J.R. LAST, B. LAUNDY, L. LAURO-TARONI, M. LAVEYRY, K. LAWSON[11], M. LENNHOLM, J. LINGERTAT[22], R.N. LITUNOVSKI, A. LOARTE, R. LOBEL, P. LOMAS, M. LOUGHLIN, C. LOWRY, J. LUPO, A.C. MAAS[15], J. MACHUZAK[19], B. MACKLIN, G. MADDISON[11], C.F. MAGGI[23], G. MAGYAR, W. MANDL[22], V. MARCHESE, G. MARCON, F. MARCUS, J. MART, D. MARTIN, E. MARTIN, R. MARTIN-SOLIS[24], P. MASSMANN, G. MATTHEWS, H. McBRYAN, G. McCRACKEN[11], J. McKIVITT, P. MERIGUET, P. MIELE, A. MILLER, J. MILLS, S.F. MILLS, P. MILLWARD, P. MILVERTON, E. MINARDI[4], R. MOHANTI[25], P.L. MONDINO, D. MONTGOMERY[26], A. MONTVAI[27], P. MORGAN, H. MORSI, D. MUIR, G. MURPHY, R. MYRNÄS[28], F. NAVE[29], G. NEWBERT, M. NEWMAN, P. NIELSEN, P. NOLL, W. OBERT, D. O'BRIEN, J. ORCHARD, J. O'ROURKE, R. OSTROM, M. OTTAVIANI, M. PAIN, F. PAOLETTI, S. PAPASTERGIOU, W. PARSONS, D. PASINI, D. PATEL, A. PEACOCK, N. PEACOCK[11], R.J.M. PEARCE, D. PEARSON[12], J.F. PENG[16], R. PEPE DE SILVA, G. PERINIC, C. PERRY, M. PETROV[21], M.A. PICK, J. PLANCOULAINE, J.-P POFFÉ, R. PÖHLCHEN, F. PORCELLI, L. PORTE[13], R. PRENTICE, S. PUPPIN, S. PUTVINSKII[8], G. RADFORD[30], T. RAIMONDI, M.C. RAMOS DE ANDRADE, R. REICHLE, J. REID, S. RICHARDS, E. RIGHI, F. RIMINI, D. ROBINSON[11], A. ROLFE, R.T. ROSS, L. ROSSI, R. RUSS, P. RUTTER, H.C. SACK, G. SADLER, G. SAIBENE, J.L. SALANAVE, G. SANAZZARO, A. SANTAGIUSTINA, R. SARTORI, C. SBORCHIA, P. SCHILD, M. SCHMID, G. SCHMIDT[31], B. SCHUNKE, S.M. SCOTT, L. SERIO, A SIBLEY, R. SIMONINI, A.C.C. SIPS, P. SMEULDERS, R. SMITH, R. STAGG, M. STAMP, P. STANGEBY[3], R. STANKIEWICZ[32], D.F. START, C.A. STEED, D. STORK, P.E. STOTT, P. STUBBERFIELD, D. SUMMERS, H. SUMMERS[13], L. SVENSSON, J.A. TAGLE[33], M. TALBOT, A. TANGA, A. TARONI, C. TERELLA, A TERRINGTON, A TESINI, P.R. THOMAS, E. THOMPSON, K. THOMSEN, F. TIBONE, A. TISCORNIA, P. TREVALION, B. TUBBING, P. VAN BELLE, H. VAN DER BEKEN, G. VLASES, M. VON HELLERMANN, T. WADE, C. WALKER, R. WALTON[31], D. WARD, M.L. WATKINS, N. WATKINS, M.J. WATSON, S. WEBER[34], J. WESSON, T.J. WIJNANDS, J. WILKS, D. WILSON, T. WINKEL, R. WOLF, D. WONG, C. WOODWARD, Y. WU[35], M. WYKES, D. YOUNG, I.D. YOUNG, L. ZANNELLI, A. ZOLFAGHARI[19], W. ZWINGMANN

[1] Harwell Laboratory, UKAEA, Harwell, Didcot, Oxfordshire, UK.
[2] Risø National Laboratory, Roskilde, Denmark.
[3] Institute for Aerospace Studies, University of Toronto, Downsview, Ontario, Canada.
[4] ENEA Frascati Energy Research Centre, Frascati, Rome, Italy.
[5] University of Leicester, Leicester, UK.
[6] Oak Ridge National Laboratory, Oak Ridge, TN, USA.
[7] Royal Institute of Technology, Stockholm, Sweden.
[8] I.V. Kurchatov Institute of Atomic Energy, Moscow, Russian Federation.
[9] Queens University, Belfast, UK.
[10] University of Essex, Colchester, UK.
[11] Culham Laboratory, UKAEA, Abingdon, Oxfordshire, UK.
[12] Imperial College of Science, Technology and Medicine, University of London, London, UK.
[13] University of Strathclyde, Glasgow, UK.
[14] Keldysh Institute of Applied Mathematics, Moscow, Russian Federation.
[15] FOM-Institute for Plasma Physics "Rijnhuizen", Nieuwegein, Netherlands.
[16] Institute of Plasma Physics, Academia Sinica, Hefei, Anhui Province, China.
[17] National Institute for Fusion Science, Nagoya, Japan.
[18] Soltan Institute for Nuclear Studies, Otwock/Świerk, Poland.
[19] Plasma Fusion Center, Massachusetts Institute of Technology, Boston, MA, USA.
[20] Nuclear Engineering Laboratory, Lappeenranta University, Finland.
[21] A.F. Ioffe Physico-Technical Institute, St. Petersburg, Russian Federation.
[22] Max-Planck-Institut für Plasmaphysik, Garching, Germany.
[23] Department of Physics, University of Milan, Milan, Italy.
[24] Universidad Complutense de Madrid, Madrid, Spain.
[25] North Carolina State University, Raleigh, NC, USA.
[26] Dartmouth College, Hanover, NH, USA.
[27] Central Research Institute for Physics, Budapest, Hungary.
[28] University of Lund, Lund, Sweden.
[29] Laboratorio Nacional de Engenharia e Tecnologia Industrial, Sacavem, Portugal.
[30] Institute of Mathematics, University of Oxford, Oxford, UK.
[31] Princeton Plasma Physics Laboratory, Princeton University, Princeton, NJ, USA.
[32] RCC Cyfronet, Otwock/Świerk, Poland,
[33] Centro de Investigaciones Energéticas, Medioambientales y Tecnológicas, Madrid, Spain.
[34] Freie Universität, Berlin, Germany.
[35] Insitute for Mechanics, Academia Sinica, Beijing, China.